

RESEARCH ARTICLE

A high-resolution climatological study of explosive cyclones in the Mediterranean region: Frequency, intensity and synoptic drivers

Cosimo Enrico Carniel¹  | Antonio Ricchi^{2,3}  | Rossella Ferretti^{2,3}  |
Gabriele Curci^{2,3}  | Mario Marcello Miglietta⁴  | Marco Reale⁵  | Piero Serafini² |
Evan David Wellmeyer² | Silvio Davolio^{6,7}  | Dino Zardi¹  | Lakshmi Kantha⁸ 

¹DICAM-Department of Civil, Environmental and Mechanical Engineering, University of Trento, Trento, Italy

²Department of Physical and Chemical Sciences, L'Aquila, Italy

³CETEMPS (Center of Excellence in Telesensing of Environment and Model Prediction of Severe Events), L'Aquila, Italy

⁴Institute of Atmospheric Sciences and Climate (CNR-ISAC), National Research Council of Italy, Padua, Italy

⁵Istituto Nazionale di Oceanografia e di Geofisica Sperimentale – OGS, Trieste, Italy

⁶Institute of Atmospheric Sciences and Climate (CNR-ISAC), National Research Council of Italy, Bologna, Italy

⁷Dipartimento di Scienze Della Terra 'A. Desio', Università degli Studi di Milano, Milan, Italy

⁸University of Colorado, Boulder, Colorado USA

Correspondence

Antonio Ricchi, Department of Physical and Chemical Sciences - CETEMPS, University of L'Aquila, Via Vetoio, L'Aquila 67100, Italy.
Email: antonio.ricchi@univaq.it

Present address

Cosimo Enrico Carniel, IAC - Institute for Atmospheric and Climate Science, ETH Zürich, Zürich, Switzerland

Funding information

This work was supported by National Centre for HPC, Big Data and Quantum Computing - PNRR Project, funded by the European Union - Next Generation EU and by the activity of COST action CA19109 MedCyclones (European network for Mediterranean cyclones in weather and climate, CA19109); Special Project ASIM-CPL funded by ECMWF. Dr. Antonio Ricchi (University of L'Aquila/CETEMPS) is funded by PON-DM1062 Project. Special thanks to Emmanouil Flaounas for providing the initial tracking dataset (Flaoun; European Union - Next Generation EU; PON-DM1062 Project)

Abstract

In the complex context of climate change and in a heavily populated area like the Mediterranean region, understanding and studying explosive cyclones (ECs) is crucial because of their potential to cause extreme weather events, including strong winds, heavy rainfall, and significant disruptions to human activities and infrastructure, as happened in 2018 with the Vaia storm. The genesis and persistence of ECs, characterized by a rapid drop in central mean sea level pressure exceeding 12 hPa in 12 hours, are influenced by various physical processes and while water vapour convergence in the mid-low troposphere is crucial, mid-upper tropospheric cyclonic vorticity advection and upper tropospheric divergence also play significant roles. In this study, we used ERA5 hourly data of mean sea level pressure from 1979 to 2020 to analyse EC occurrences in the Mediterranean. The identification of EC events followed the 12-hr deepening-rate criterion introduced by Zhang et al. (2017), as shorter deepening rates definitions proved unreliable. A total of 80 ECs were identified and classified based on their spatial occurrence and magnitude, 34 of which were concentrated in the northwest of the basin, likely due to orographic deformation caused by the Alps on baroclinic waves originating from the Atlantic. The study also identified recurring synoptic patterns associated with the persistence of ECs over the sea, including the presence of potential vorticity (PV) streamers and mid-tropospheric dry-air intrusions. Empirical Orthogonal Function (EOF) analysis highlighted the Scandinavian pattern as the primary driver, with blocking conditions over western Russia and Scandinavia, and composite analyses revealed the intrusion of PV to various atmospheric levels, extending up to 500 hPa. In summary, this study offers valuable insights into the complex mechanisms governing EC formation in the Mediterranean Basin, shedding light on the synoptic patterns, atmospheric dynamics, and potential impacts on regional weather systems.

KEYWORDS

atmospherical tides, climatological analysis, deepening rate, explosive cyclones, Mediterranean Basin, physical phenomenon, severe weather

This is an open access article under the terms of the [Creative Commons Attribution](https://creativecommons.org/licenses/by/4.0/) License, which permits use, distribution and reproduction in any medium, provided the original work is properly cited.

© 2024 The Author(s). *Quarterly Journal of the Royal Meteorological Society* published by John Wiley & Sons Ltd on behalf of Royal Meteorological Society.

1 | INTRODUCTION

In a time of growing concern related to the potential impacts of climate change, the ability to understand and forecast severe meteorological events becomes even more critical for the welfare of the general public. Particularly intense phenomena such as heavy precipitation, heat waves, windstorms, marine storms and storm surges need to be predicted in time to be properly managed. Their consequences directly affect the agricultural/production sector, the industrial sector, transport-related infrastructure, communications and the energy sector. Last but certainly not least, they pose a direct risk to the safety and well being of millions of people.

Among the weather hazards, explosive cyclones (ECs, hereafter) are an example of relatively rare (1 in 50 cyclones is an EC), but potentially highly destructive events. ECs occur prevalently in winter (Allen et al., 2010; Wang & Rogers, 2001; Reale et al., 2019), have a typical life cycle of 2–5 days and a horizontal scale of 2000–3000 km over mid-latitude oceans (Zhang et al., 2021). They can cause extensive devastation due to the strong winds and torrential rains associated with them, resulting in severe losses in terms of human life and property. They were originally defined by Tor Bergeron between 1940 and 1950 as low-pressure systems exhibiting a deepening rate (DR) of at least 1 Bergeron unit, that is, at least 24 hPa in 24 hours. This definition was further refined by Sanders and Gyakum (1980), that geostrophically adjusted it to a reference latitude (in their study set at 60° N). Roebber (1984) carried out a statistical analysis of ECs, showing that they are not different in their location of genesis compared to other extratropical cyclones and more recently, Zhang et al. (2017) observed that the highest frequency of ECs occurred in the 35–50° N latitude range and hence they redefined the DR of 1 Bergeron as a decrease in the central pressure of 12 hPa in 12 hours when adjusted geostrophically to a mean reference latitude of 45° N.

One of the most important physical processes that contribute to the genesis and maintenance of ECs is water vapour convergence in the mid-low troposphere (Zhang et al., 2021). However, cyclonic vorticity advection in the mid-upper troposphere and divergence in the upper troposphere play a primary role as well, together with baroclinic instability in the triggering phase (Karacostas & Flocas, 1983; Manobianco, 1989; Sanders, 1986; Wash et al., 1992). Several other mechanisms come into play throughout their development and their exceptionally rapid intensification (which is the primary characteristic and difference with other extratropical cyclones), including strong upper-level PV anomalies (Bosart & Lin, 1984; Reader & Moore, 1995; Uccellini et al., 1990; Zehnder &

Keyser, 1991), intrusions of stratospheric dry air, air–sea interactions, latent heat release (Anthes et al., 1983; Emanuel et al., 1987; Gall, 1976; Gyakum, 1983; Mullen & Baumhefner, 1988), and warm-air advection. Diabatic heating is the most dominant since without its contribution the intensification rate would be much lower and certainly not in the ‘explosive’ range (Ahmadi-Givi et al., 2004; Liberato et al., 2013).

In the last decades, with the advent of observational satellite and modelling technologies, many studies demonstrated the possible formation of ECs over the Mediterranean Basin (MB), where the complex topography and the presence of low-level vorticity features may favor cyclone development, particularly through lee cyclogenesis in the Gulf of Genoa (Buzzi et al., 2020; Buzzi & Tibaldi, 1978), cutoffs of Atlantic baroclinic waves and Tropical-Like Cyclones (TLC; Miglietta & Rotunno, 2019; Miglietta et al., 2021). Several works showed that the explosive deepening of these events is mostly driven by the interaction of low and high-level positive PV anomalies (Davalio et al., 2020; Lionello et al., 2006) or sustained by air–sea interaction (Flaounas et al., 2022), while other works highlighted the rarity of their occurrence in this basin, producing the first climatologies of ECs (Conte, 1986; Conte et al., 1997). Later on, some exceptionally disruptive events of this sort were analysed by Karacostas and Flocas (1983) and Lagouvardos et al. (2007).

More recently, Kouroutzoglou et al. (2011) have summarised EC climatology in the MB by using an automatic tracking algorithm implemented by the University of Melbourne (Murray & Simmonds, 1991a, 1991b; Simmonds & Murray, 1999), using 6-h ERA-40 Reanalysis data of the ECMWF (Uppala et al., 2005) for the period 1962–2001 and with a spatial resolution of $2.5^\circ \times 2.5^\circ$ and using Sanders and Gyakum (1980)’s 24 h. definition. With these methods, their analysis produced a climatology of over 200 ECs, that is, 5.5 yearly occurrences on average and a clear seasonal preference, with winter witnessing approximately 55% of the events, peaking in December. Three specific regions were identified as conducive to EC development: the north Adriatic Sea and the Tyrrhenian Sea, the Aegean Sea, and northwestern Africa. Notably, differences between Western Mediterranean (WM) and Eastern Mediterranean (EM) ECs were observed, with EM cyclones being less frequent yet more intense. Furthermore, the study highlighted the movement patterns of these cyclones, indicating a tendency to form in WM, dissipating either in the area of Southern Italy or following an eastward trajectory towards EM.

Using the high-resolution ERA5 Reanalysis dataset by ECMWF (Hersbach et al., 2020) for the period 1979–2020, the present study investigates in detail the occurrence of ECs formed in the Mediterranean Sea area, intending to

determine their frequency, temporal trend, and the most typical synoptic patterns associated with these disruptive events. The employment of high spatial ($0.25^\circ \times 0.25^\circ$) and hourly resolution data from ERA5, together with the use of a recently developed method of track detection (Flaounas et al., 2023), conceived to compare 10 different algorithms and build the first reference tracks dataset, constitutes a significant novelty for this type of work in the Mediterranean region. Exploiting the higher temporal resolution (compared to previous climatologies) the study also explores different methods to compute DR and evaluates which of them allows a more coherent identification of ECs in the region. In summary, this work fills a crucial gap in Mediterranean ECs research by providing higher resolution data and advanced tracking methods, offering unprecedented accuracy in understanding their behaviour, which is essential for improving regional forecasting and mitigating the impacts of these disruptive weather events. Moreover, a crucial finding of this work is the prominent influence of solar atmospheric tides on the detection process of ECs, particularly in northern Africa, which was never considered in previous papers. These tides distort the DR signal, leading to frequent misdetections of EC in the region.

A detailed discussion of the data used in the work and the methods utilized in the analysis are described in Section 2. *Data and Methods*, while a thorough explanation of the DR computation testing is provided in Section 3. The

results and their explanation are contained in Section 4. *Results*, leading to the final remarks in Section 5. *Discussion and Conclusions*.

2 | DATA AND METHODS

2.1 | Data source and cyclones tracking algorithm

For reconstruction of the cyclone activity in the MB, an objective detection and tracking procedure was applied to the $0.25^\circ \times 0.25^\circ$ hourly mean sea level pressure (MSLP) from the ECMWF ERA5 Reanalysis dataset, which covers all years in the period 1979–2020 (Hersbach et al., 2020; Hersbach et al., 2023). An ensemble of 10 different tracking algorithms from the work of Flaounas et al. (2023) was employed to retrieve cyclone tracks. In their study, these algorithms use essentially three parameters: the MSLP, the relative vorticity field at 850 hPa, and the geopotential height at 1000 hPa level. Their combination builds datasets for cyclone tracks of ranked confidence level using the 10 different outputs, offering greater confidence in identifying cyclones and their dynamic life stages (from formation to dissipation) compared to individual methods. In this study, we select composite tracks with a confidence level of 5, denoting concurrence among at least five out of 10 cyclone detection algorithms.

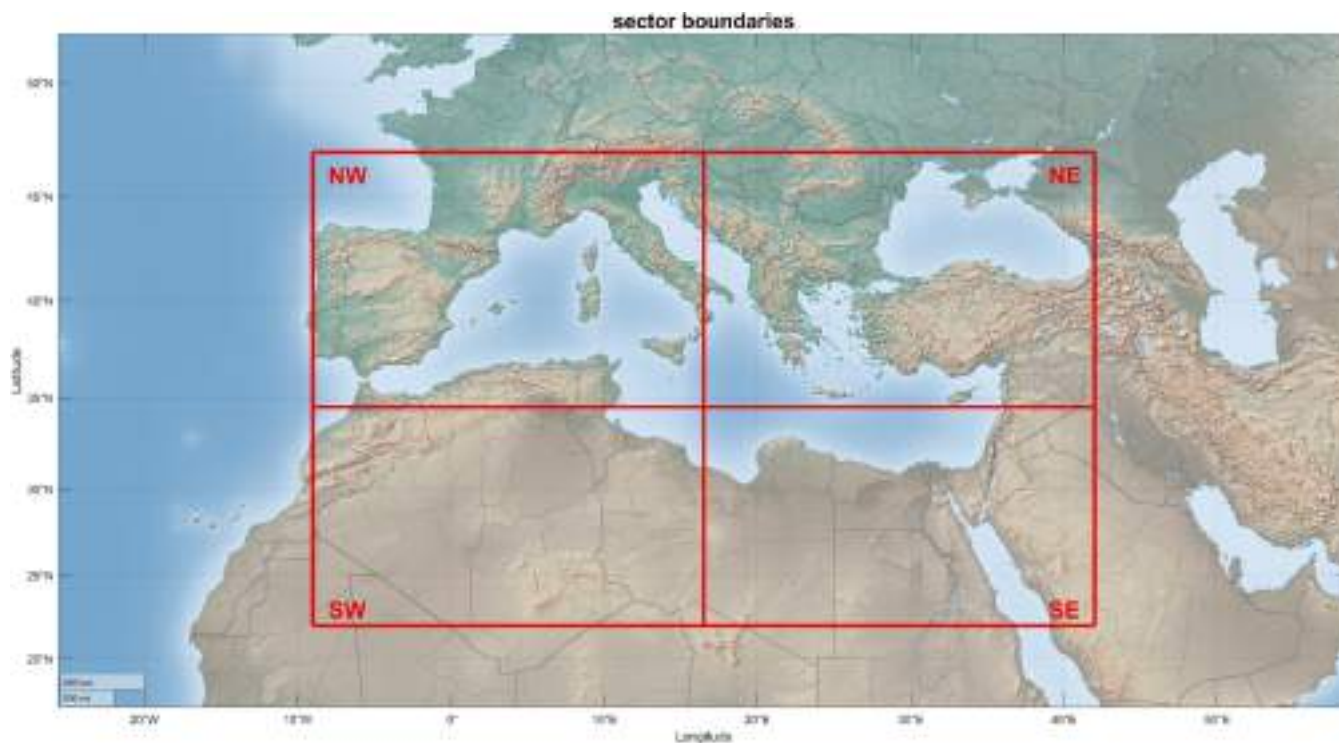


FIGURE 1 The four sectors as specified in Table 1.

TABLE 1 List of sector boundaries selected as subdomains of the Mediterranean Basin (MB) and in four main areas of interest, considered representative of the MB for cyclone development of explosive cyclones that are reported in Table 2.

Sector	Latitude range	Longitude range
SW	22–34.5° N	9° W–16.5° E
SE	22–34.5° N	16.5–42° E
NW	34.5–47° N	9° W–16.5° E
NE	34.5–47° N	16.5–42° E

2.2 | Research area

The base dataset covers a rectangular domain defined as 20–50° N and 20° W–45° E (Flaounas et al., 2023) with a total of 7021 cyclones. Because of interest exclusively in the ECs' effects in the Mediterranean Sea, the initial dataset was restricted by considering only the cyclones that develop inside the domain, even if they might be generated outside of the basin, thus excluding cyclones that occur exclusively in the Atlantic, the Baltic Sea and in the northern part of the continent. This translates into the average latitude and average longitude of the track being contained within the limits of the chosen domain, which is set to longitude [0°, 37°] and latitude [25°, 45°] (Figure 1).

In addition, this domain is further divided into four quadrants, as performed by Lionello et al. (2016), described in Table 1.

The minimum longitude of 0° was chosen to exclude the Bay of Biscay, an oceanic region on the border with France where Atlantic cyclones are often detected. These cyclones sometimes move into the MB, but hardly affect it for a long duration or with relevant impact in the area and have therefore been excluded from the analysis. Moreover, cyclones with a lifespan of less than six hours were excluded. Once these filters have been applied to the domain, the remaining cyclones are 3341.

2.3 | Methods

In the analyses of cyclone intensification, starting from *Tor Bergeron* (Sanders and Gyakum, 1980; Zhang et al., 2017, 2021), the DR of central sea level pressure (CSLP) has been used to characterise the rate of intensification of the cyclone and not the most appropriate differential pressure p (i.e., the pressure difference between the centre and the edge of the cyclone). However, assuming geostrophic balance holds

$$fV = \frac{1}{\rho} \left(\frac{\partial p}{\partial r} \right), \quad (1)$$

where is the air density, the geostrophic velocity V depends on both the radial pressure gradient $\partial p / \partial r$ and the Coriolis parameter $2\Omega \sin \phi$, where ϕ is the latitude. Since the velocity characterises the cyclone intensity, the cyclone intensification rate can be estimated from:

$$\frac{dV}{dt} \sim - \left(\frac{1}{\sin \phi} \right) \frac{d(\Delta p)}{dt}, \quad (2)$$

where Δp is the pressure difference between the centre and the outskirts of the cyclone. However, it is common to replace Δp by p_c , the CSLP. The distinction between Δp and CSLP is important to keep in mind, since atmospheric tides modulate the pressure felt at the Earth's surface, as discussed in Section 3. In accordance with Equation (2), DR is usually normalised with the latitude of the cyclone by referencing it to a chosen reference latitude. This takes into account the fact that the same radial pressure gradient gives rise to a higher (lower) velocity at lower (higher) latitudes. Sanders and Gyakum (1980) chose 60° as the reference latitude and defined the unit of DR in terms of Bergeron, that is, the deepening rate of 1 hPa·hr⁻¹ (or equivalently 24 hPa in 24 hours) at 60° latitude. On the other hand, Zhang et al. (2017, 2021) chose 45° as the reference latitude so that DR in Bergeron is given by

$$\text{DR} = \left(\frac{p_{t-6} - p_{t+6}}{12} \right) \left[\frac{\sin 45^\circ}{\sin \left(\frac{\phi_{t-6} + \phi_{t+6}}{2} \right)} \right], \quad (3)$$

where a 12-hr difference in CSLP is used to compute the DR, instead of the 24-hr difference used by Sanders and Gyakum (1980). Note that, for simplicity, we have dropped the subscript c from the pressure term. Here again, 1 Bergeron is 1 hPa·hr⁻¹, or 12 hPa in 12 hours, at 45° latitude.

When higher resolution data (such as hourly) of cyclone CSLP are available, in view of the shorter lifetime of some ECs, a more general expression to compute the DR over an arbitrary period can be defined:

$$\text{DR} = \left(\frac{p_{t-\tau/2} - p_{t+\tau/2}}{12} \right) \left[\frac{\sin 45^\circ}{\sin \left(\frac{\phi_{t-\tau/2} - \phi_{t+\tau/2}}{2} \right)} \right], \quad (4)$$

where t indicates the present timestep and τ the total timespan of the DR computation. The analysis is performed by using $\tau=12$ -hr DR. However, in the MB and many other regions, cyclones can have even shorter life-spans (Lionello et al., 2016), and as such, it is tempting to explore higher temporal resolution definitions of Bergeron, such as the equivalent 6-hr DR of 6 hPa in 6 hours,

since hourly CSLP data are available from the dataset. This availability makes it possible to choose a smaller interval and calculate 2-hr, 4-hr, 6-hr and 12-hr DR using the more general expression. We will examine and comment on this possibility in this study.

Once the ECs are detected, the study also aims at characterising the typical synoptic patterns explaining their occurrence in the MB, which is performed with the Empirical Orthogonal Functions (EOF) analysis, implemented with the help of the Python *EOF* package (Dawson, 2016). This analysis involves three distinct datasets:

1. Explosive dataset: ERA5 data of MSLP in the domain 25–70° N, 60° E–60° W, but restricted to the time steps at which each of the ECs identified reaches the absolute maximum value of DR, that is, its maximum intensification.
2. Random dataset: ERA5 data of MSLP in the domain 25–70° N, 60° E–60° W but restricted to the time steps at which 80 randomly selected cyclones (independently of their DR) reach their absolute maximum value of DR (which, in this case, will not necessarily surpass the 1 Bergeron threshold). Since the cyclones are randomly selected, this dataset also includes 1 EC with $DR > 1$ Bergeron.
3. Intense dataset: ERA5 data of MSLP in the domain 25–70° N, 60° E–60° W but restricted to the time steps at which the 80 most intense cyclones (by minimum pressure reached) attain their minimum central pressure.

To account for the change in distance of the meridians in the south–north direction (area weighting), the square root of the cosine of latitude is applied to each grid point before the computation of EOF.

As a further evaluation, since stratospheric dry-air intrusions (SDIs) and upper- and lower-level PV anomalies are known to contribute significantly to the triggering and intensification of extratropical cyclones at mid-high latitudes (Anthes et al., 1983; Bosart & Lin, 1984; Emanuel et al., 1987; Gall, 1976; Gyakum, 1983; Mullen & Baumhefner, 1988; Sinclair et al., 2020; Uccellini et al., 1985), we investigate whether they play a similar role in the intensification of ECs in the MB. To accomplish this task, we carried out a composite analysis. After identifying the position of each cyclone at its point of maximum DR, a matrix was created for each cyclone, representing a domain of 3000×3000 km (approximately 27°), with the cyclone centre set as the central point. The composite mean field was obtained by averaging these matrices, providing a representative structure of the cyclones based on PV and relative-humidity (RH) data.

Additionally, we explore the role of mean surface latent heat (MLHF) and mean surface sensible heat (MSHF) fluxes in the intensification of ECs. For this analysis, we extracted the maximum values of PV, MLHF, and MSHF, and the minimum values of RH, within a circular domain of 250 km radius around each cyclone's centre.

The decision of choosing this method rather than taking the average within the radius is motivated by the need to capture the most significant anomalies, which might be concentrated in a small portion of the cyclone's vicinity. Averaging would dilute these extreme values with the surrounding 'background' values, making it difficult to discern the true intensity of the anomaly and to accurately compare ECs with random ones.

Both these analyses employ ERA5 Reanalysis data at a $0.25^\circ \times 0.25^\circ$ resolution, specifically:

- Hourly data at 350, 500, and 850 hPa levels for PV and RH in the composite analysis.
- Hourly data at single levels for MLHF and MSHF for each cyclone at the time of maximum DR, extracting values within a circular area of a 250 km radius around the cyclone's centre on that specific date.

3 | EXPLOSIVE-CYCLONE DETECTION AND COMPUTATION OF THE DEEPENING RATE

Figure 2a,b shows the DR for a cyclone over North Africa (EC6019) and over the Mediterranean Sea (EC821), respectively. Both 2-hr and 6-hr DRs exhibit oscillations with a period of roughly 12 hours, with higher amplitudes (~ 2 hPa) for the cyclone over North Africa than that over the Mediterranean Sea (~ 1 hPa). On the other hand, both 12-hr DR and the 12-hr running mean of 2-hr DR are almost identical and are devoid of such oscillations, which, as will be thoroughly discussed below, derive from solar semidiurnal atmospheric tides. Figure 3 shows plots obtained by aligning one of the oscillation peaks of the DR for the 10 most intense cyclones (i.e., the 10 with the maximum value of DR), to highlight the periods of oscillation. In the top panel the 10 most intense cyclones over North Africa and in the bottom panel the 10 most intense over the Mediterranean Sea are shown. The presence of the tidal signal in the DR hourly values at a roughly 12-hr period is recorded in both areas, but at somewhat higher amplitudes over land. Daytime solar heating and subsequent night-time cooling of the Earth's surface modulates the surface pressure and gives rise to solar semidiurnal (S_2) and solar diurnal (S_1) tidal

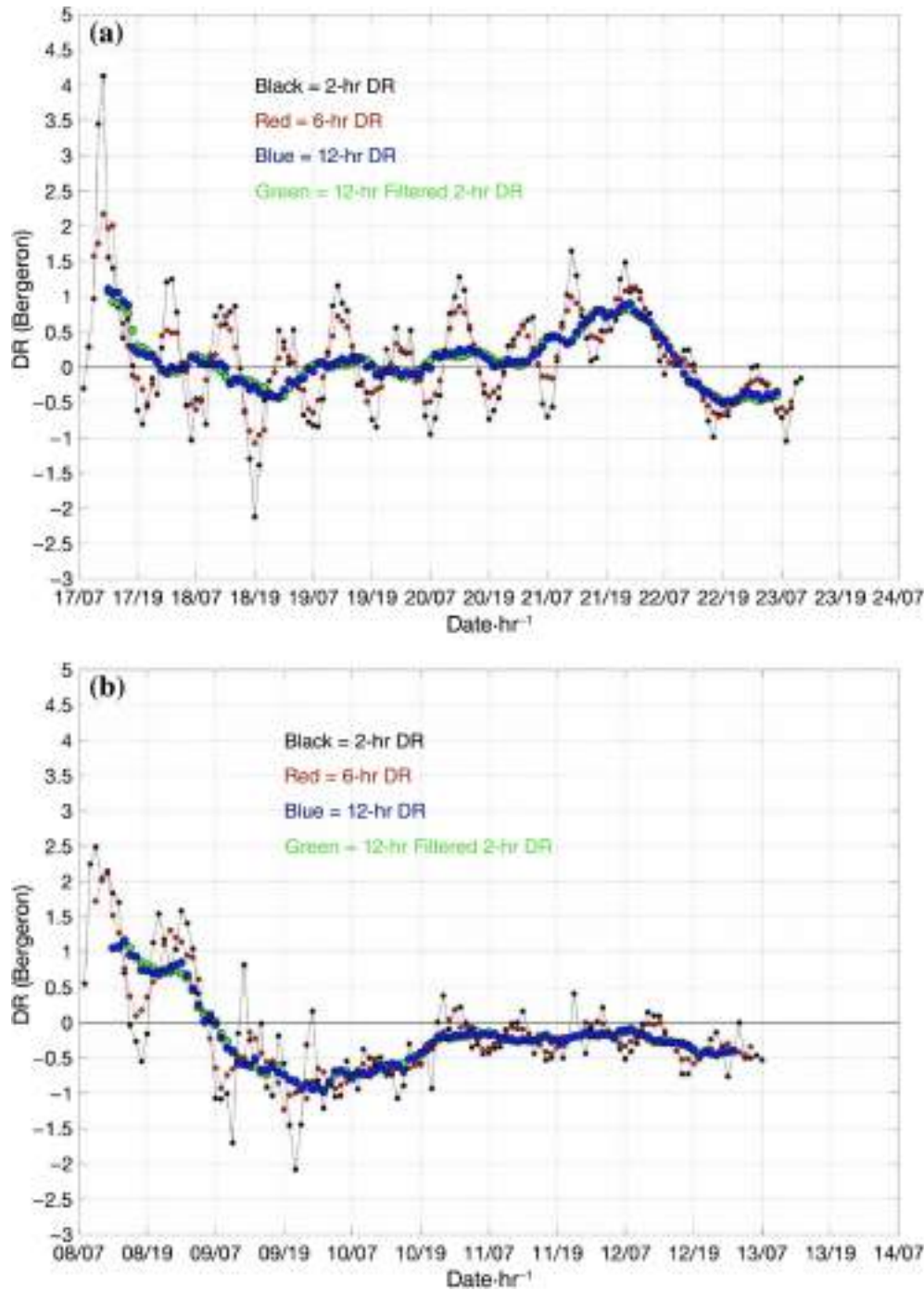


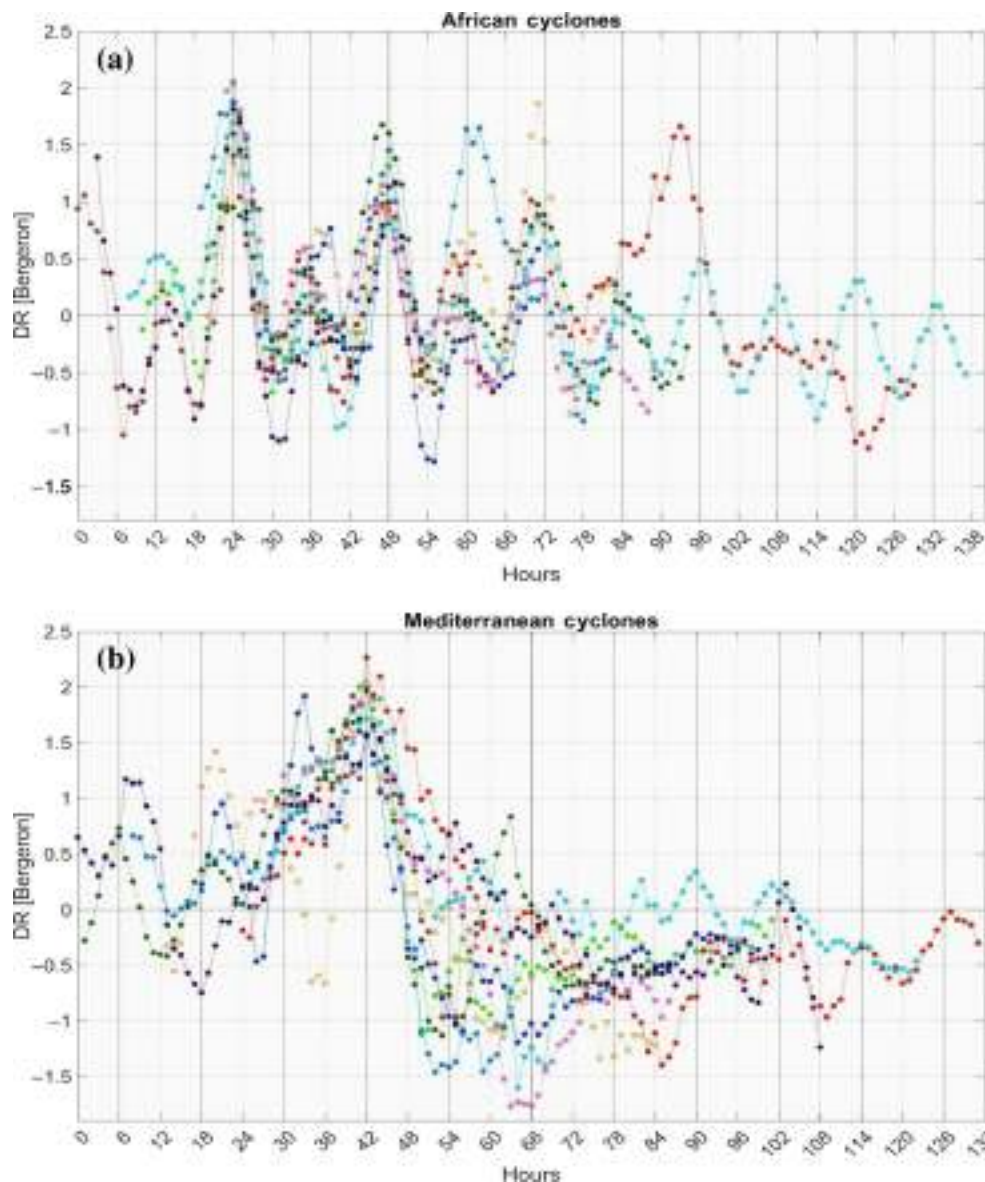
FIGURE 2 Time series of 2-hr (black), 6-hr (red) and 12-hr (blue) deepening rates (DR, in Bergeron). In both figures, the 12-hr running mean of 2-hr DR is shown in green. (a) For a typical cyclone (EC6019) over North Africa; (b) for a typical cyclone (EC821) over the Mediterranean Sea.

fluctuations at exactly 12- and 24-hr periods, respectively (Covey et al., 2011; Schindelegger & Ray, 2014). Figure 11 of Schindelegger and Ray (2014) shows principally latitudinally varying S_2 sea level pressure, with amplitudes decreasing from the equatorial regions (roughly 1.2 to 1.5 hPa) to polar regions (0 to 0.2 hPa). In the Mediterranean region, S_2 amplitudes are around 0.6–0.8 hPa. Their Figure 10 shows diurnal S_1 tides with amplitudes up to 1.8 hPa, with higher values generally over land, especially near the Equator. S_1 amplitudes are quite small (0 to 0.4 hPa) over the oceans. Naturally, stronger

diurnal heating leads to higher S_1 amplitudes over land than over water. In our study region, S_1 amplitudes are rather small (<0.2 hPa). As such, we expect to see predominantly semidiurnal S_2 signals in the cyclone CSLP.

S_2 modulates the pressure everywhere in the cyclone, hence does not contribute to the differential pressure responsible for cyclone winds, as long as the size of the cyclone is sufficiently small compared to the scale of variation of tides. If the analysis of the DR is based on the differential pressure Δ the tidal signal is automatically

FIGURE 3 (a) Cumulative plot of diurnally aligned deepening-rate (DR) trend in the case of the 10 most intense cyclones that occurred over North Africa. Note that the signal of S_2 tide is readily visible, roughly at a 12-hr period. (b) Same as the first panel but for the 10 most intense cyclones that occurred over the Mediterranean Sea. Note that the S_2 tidal signal is still present, but less prominent.



cancelled out. However, most (if not all) studies use cyclone CSLP, which is modulated and hence corrupted by solar tides.

Because of contamination principally by S_2 , 6-hr DR mistakenly detected more than 800 cyclones reaching 1 Bergerson at some point during their lifetime, more than half occurring over North Africa (see Figures S2 and S3). These cyclones undergo a moderate decrease of pressure in relatively high-pressure surroundings, which makes the 6-hr algorithm detect them as EC while, from a physical standpoint, they are not (see Section 5 for more information).

Since we established that spurious tidal signals corrupt the DR at higher temporal resolutions, we have used a 12-hr DR henceforth in our study (i.e., Equation 3), as it produces results consistent with the previous literature on cyclone explosive intensification in the MB.

4 | RESULTS

4.1 | Overview of cyclonic phenomena in the Mediterranean Basin

The probability of any type of cyclone crossing the different regions of the MB (Figure 4) shows how the distribution of ECs in the MB differs from the general distribution of cyclones. This plot is built up by accounting for all the cyclonic events present in the initial dataset and counting every cyclone crossing each cell of the $0.5^\circ \times 0.5^\circ$ resolution grid over the domain only once, even if the initial dataset contains several passages of it over the same cell. Cells are left blank if the percentage is less than 0.1%.

The distribution of cyclone probability is consistent with that highlighted in earlier studies (Flaounas et al., 2018; Flaounas et al., 2022; Lionello et al., 2016;

Reale et al., 2022), with two large activity locations standing out: the first covers the Gulf of Genoa and the northern Tyrrhenian Sea, with 9% maximum probability, and a total of 463 cyclones (11 of these are ECs) crossing the area. The probability decreases approaching Sicily and the Ionian Sea (3%–4%). In the entire Ionian Sea, there are a total of 1159 cyclones (26 of these are ECs). The area of Cyprus and the Aegean Sea shows another maximum (9% as well) featuring the passage of 553 cyclones (eight of these are ECs). Another secondary maximum covers the Adriatic Sea, with lower values of probability (4%–5%). A statistical summary divided per area is provided in Table S1.

The vast majority of events occur over the sea in the aforementioned areas, but there are also inland regions with some activity, such as North Africa, near the Atlas Mountains, the central part of Spain and the regions on the northern side of the Black Sea (1%–3%).

4.2 | Explosive cyclones detected with 12-hr deepening rate

With the 12-hr DR methodology, 80 cyclones were identified as ECs using the 12-hr DR methodology, a smaller number compared to the 222 identified in Kouroutzoglou et al., 2011. Figure 5 shows the probability of an EC crossing each cell of the grid and the main hotspots overlap

with the general case discussed in Figure 4, in particular the Gulf of Genoa and the area of the Cyprus low (in both cases up to 12% and in accordance with previous studies). Additional areas of intense activity cover the Ionian Sea, with clusters near the coasts of Tunisia and Libya (8%–10%), the Tyrrhenian Sea, connected with a storm track starting from the Balearic Islands, and the Adriatic Sea in which the highest probability is reached near the coasts of the Apulia region of Italy (8%–10%). As in the general case, ECs are located primarily over the sea, but isolated areas of activity are also visible in the Northern African region (Libya, Tunisia, Morocco, and the Atlas Mountains) and near the Black Sea.

Identifying as the starting point the first step of each EC inside the area, six cyclones originate in the Gulf of Genoa (over a total of 11 entering the area, so possibly triggered in other locations), two in the area of Cyprus and the Aegean Sea (where there is the passage of eight ECs), seven in the entire Ionian Sea (26 crossings in total) and one starts near the Balearic Islands (seven crossings in total). Note that these numbers are retrieved with the help of a search algorithm that considers the regions in Table 2.

Figure 6 shows the corresponding tracks of the ECs during their explosive deepening phase (EDP), that is, the part of the deepening characterised by a DR > 1 Bergeron. This is shown by coloured points, with colours corresponding to CSLP values, and a coloured circle at the point of maximum DR. Some ECs can undergo more than one

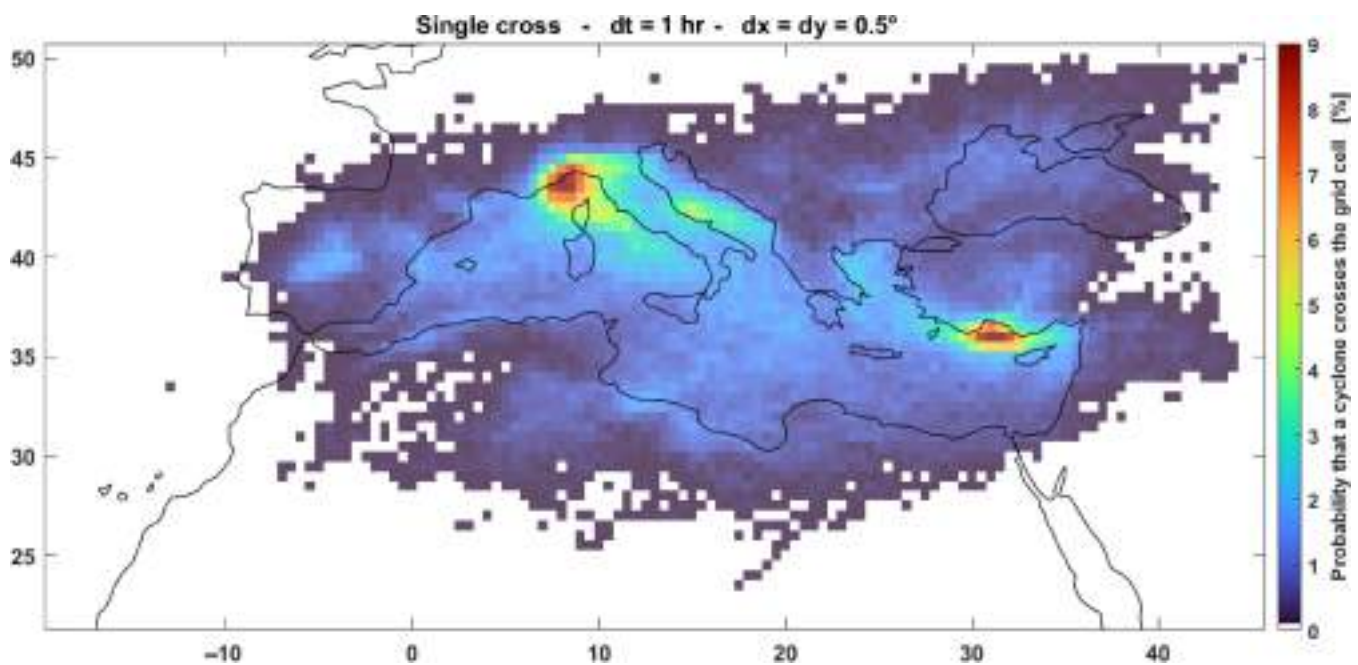


FIGURE 4 Probability of cyclones crossing the Mediterranean Basin in $0.5^\circ \times 0.5^\circ$ cells. The plot is retrieved by scanning in the complete dataset all the points where latitude and longitude are included within the boundary coordinates of the domain. Every cyclone found with this method is counted only once (single crossing) and the percentage of probability is then computed.

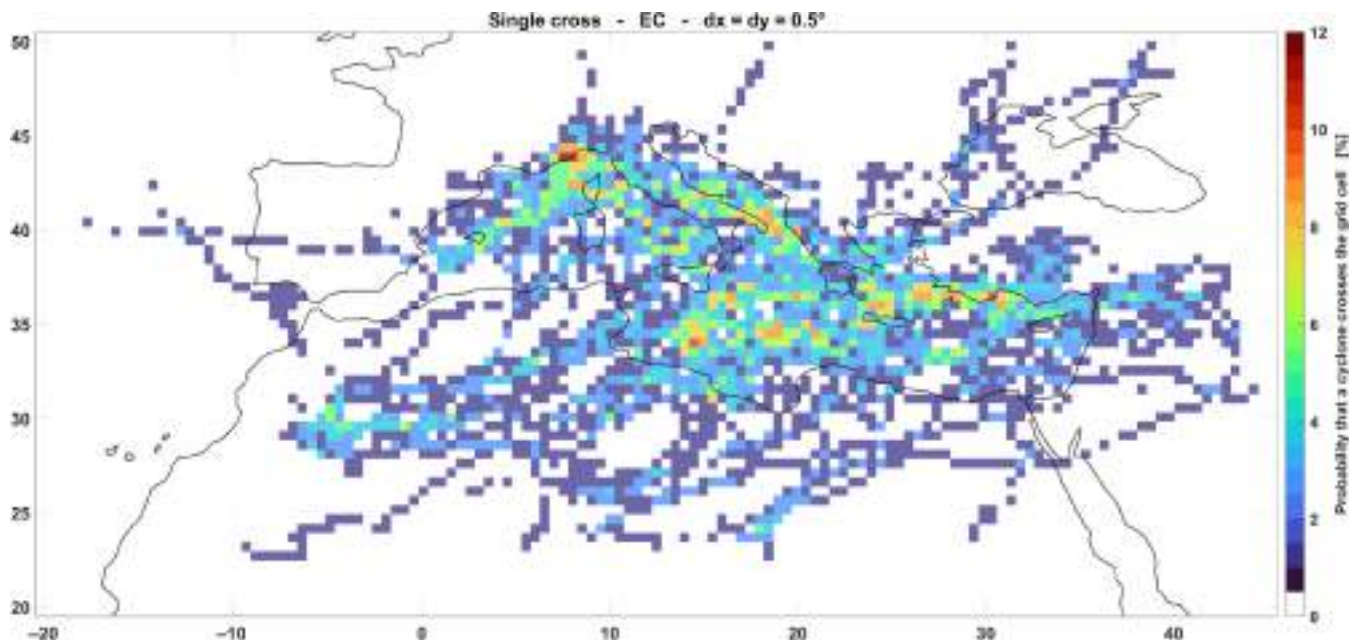


FIGURE 5 Probability of explosive cyclones (ECs) crossing each cell of the $0.5^\circ \times 0.5^\circ$ grid over the Mediterranean Basin. This plot is similar to Figure 4, but using a dataset containing only data of the ECs detected using a 12-hr deepening rate.

TABLE 2 List of areas of interest (see Figure S1).

Area	Latitude range	Longitude range
Ionian Sea	32–38.5° N	10–21° W
Balearic Islands	37.5–42° N	1.5–6° W
Aegean Sea and Cyprus	33.5–37.5° N	23–35° W
Gulf of Genoa	41.5–44.5° N	7.5–10.5° W

EDP along their tracks; however, to investigate their spatial distribution, only the phase of maximum DR was considered. Few ECs remain over North Africa but have very brief EDP, with a maximum duration of 5–6 hours. A clear indication of the key role of the air–sea interaction in the intensification process comes from the large number of cyclones undergoing explosive intensification as they reach the Mediterranean Sea.

As summarized in Table 3, the area of the Balearic Islands is affected by the most intense cyclones in terms of minimum CSLP. Here the ECs reach the absolute lowest value of CSLP of 975 hPa, with an average minimum pressure of 991 hPa (computed as the sum of the minimum pressures reached by every cyclone in the selected domain, divided by the number of cyclones), and usually move north. The duration of the EDP is, on average, 4.4 hours, with a maximum duration of 10 hours. The Ionian Sea, on the other hand, is affected mainly by cyclones born in North Africa but exhibiting their EDP over the sea, reaching an absolute minimum pressure of 985 hPa,

with a mean minimum pressure of 1000 hPa. Here the EDP durations are the longest, 6.2 hours on average and 15 hours maximum. This duration is reduced in the case of the Gulf of Genoa (on average 3.9 hours, maximum of eight hours), reaching values of mean CSLP of 1004 hPa, and a minimum value of 985 hPa. Moreover, in this confined region, 11 cyclones reach their maximum DR. In the Aegean Sea and Cyprus area the average minimum CSLP is 998 hPa, with an absolute minimum of 981 hPa, and the EDP last on average 4.1 hours, with a maximum of six hours.

4.3 | Frequency of occurrence and spatial distribution of explosive cyclones

Figure 7 shows the seasonal distribution of ECs in each of the four sectors of the MB listed in Table 1. Each cyclone is located according to the point of its track where it reaches the maximum local intensification (12-hr DR) rate. Note that the total number of cyclones displayed is not 80, but 78; this is because some do not reach their maximum DR inside any sector, despite being contained in the entire domain as explained in Section 2.2. Consistent with earlier studies (Kouroutzoglou et al., 2011; Roebber, 1984), these histograms show that ECs in MB are essentially a wintertime phenomenon; in fact 68% of ECs occur from November to February (compared to 55% in Kouroutzoglou et al., 2011), with peaks in frequency in

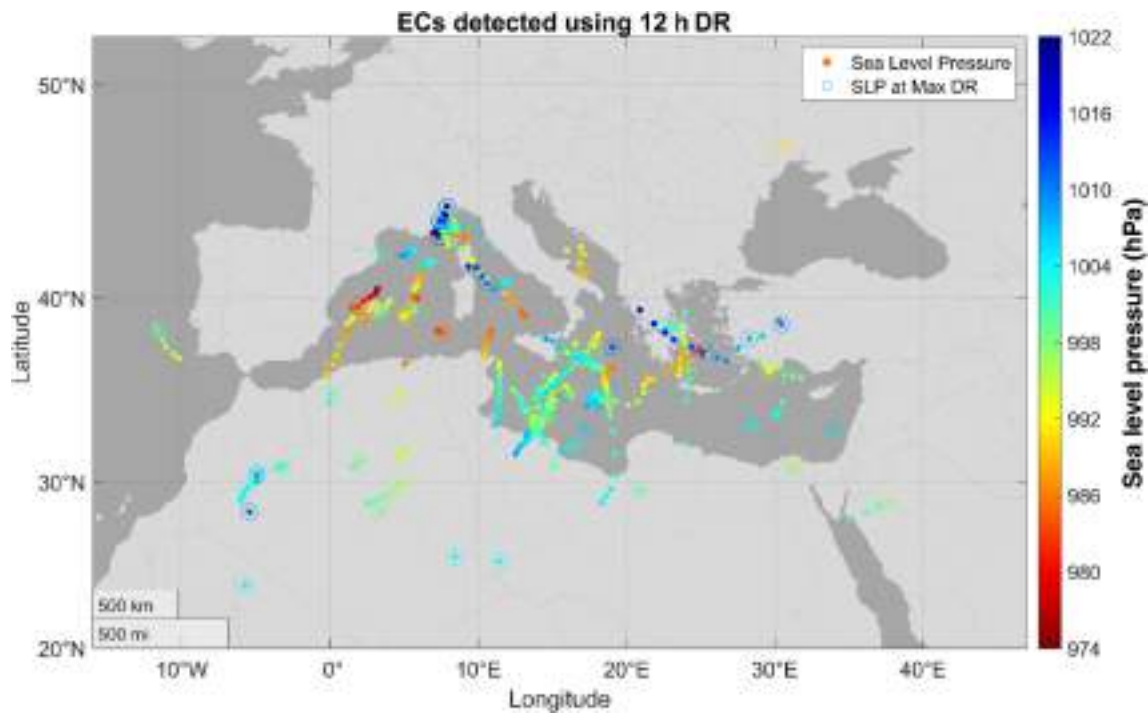


FIGURE 6 Scatterplot of the explosive deepening phase of the 80 explosive cyclones (ECs) detected using the 12-h deepening rate (DR). Coloured dots indicate the central sea level pressure (CSLP) in accordance with the colour bar, while circled dots indicate CSLP at the point corresponding to the maximum DR reached along the track of the cyclone.

TABLE 3 Summary of characteristics of ECs in the area of interest of the Mediterranean Basin.

	Ionian Sea	Balearic Island	Aegean Sea and Cyprus	Gulf of Genoa
N° EC	26	7	8	11
Mean DR [Bergeron]	0.2436	0.2239	0.2287	0.2385
Max DR [Bergeron]	1.8715	1.6898	1.5733	1.5733
Mean EDP duration [hours]	6.2	4.4	4.1	3.9
Max EDP duration [hours]	15.0	10.0	6.0	8.0
Mean CSLP [hPa]	1000.12	990.88	998.27	1003.62
Min CSLP [hPa]	984.95	974.70	980.74	985.46

Abbreviations: CSLP, central sea level pressure; DR, deepening rate; EC, explosive cyclone; EDP, explosive deepening phase.

sectors SW, NW and NE in January or February, while in the SE area the peaks occur in March.

The NW sector is the most affected (34 cases, 42.5% of the total) since it includes the Gulf of Genoa, which constitutes a hotspot for cyclone intensification, due to the unique surrounding orography and the presence of the Alps, which interact with the baroclinic waves from the Atlantic (Buzzi & Tibaldi, 1978; Buzzi et al., 2020; Speranza et al., 1985); however, the genesis of cyclones can also happen in situ. NW is followed by NE (18 cases, 22.5%), SW (17 cases, 21.25%), and SE (nine cases, 11.25%).

Overall, this distribution indicates that the northern part of the MB is the most affected with a total of 52 cyclones, 65% of the total number, which suggests that

the frequency of occurrence of maximum DR decreases moving south. This may be attributed to the lower contribution of latent heat flux in these regions, likely due to the greater presence of land.

The frequency of occurrence tends to decrease with DR's maximum in all four sectors, as shown in Figure 8. The NE sector presents the highest average intensity (1.27 Bergeron), followed by SW (1.26 Bergeron), which contains the absolute maximum value of 1.87 Bergeron, NW (1.2 Bergeron), which has the second-highest peak (1.80 Bergeron), and SE (1.06 Bergeron). This suggests that the NW sector, despite being the highest-frequency area, is not (on average) the one subjected to the strongest DRs. Additionally, the DR of ECs decreases as they move

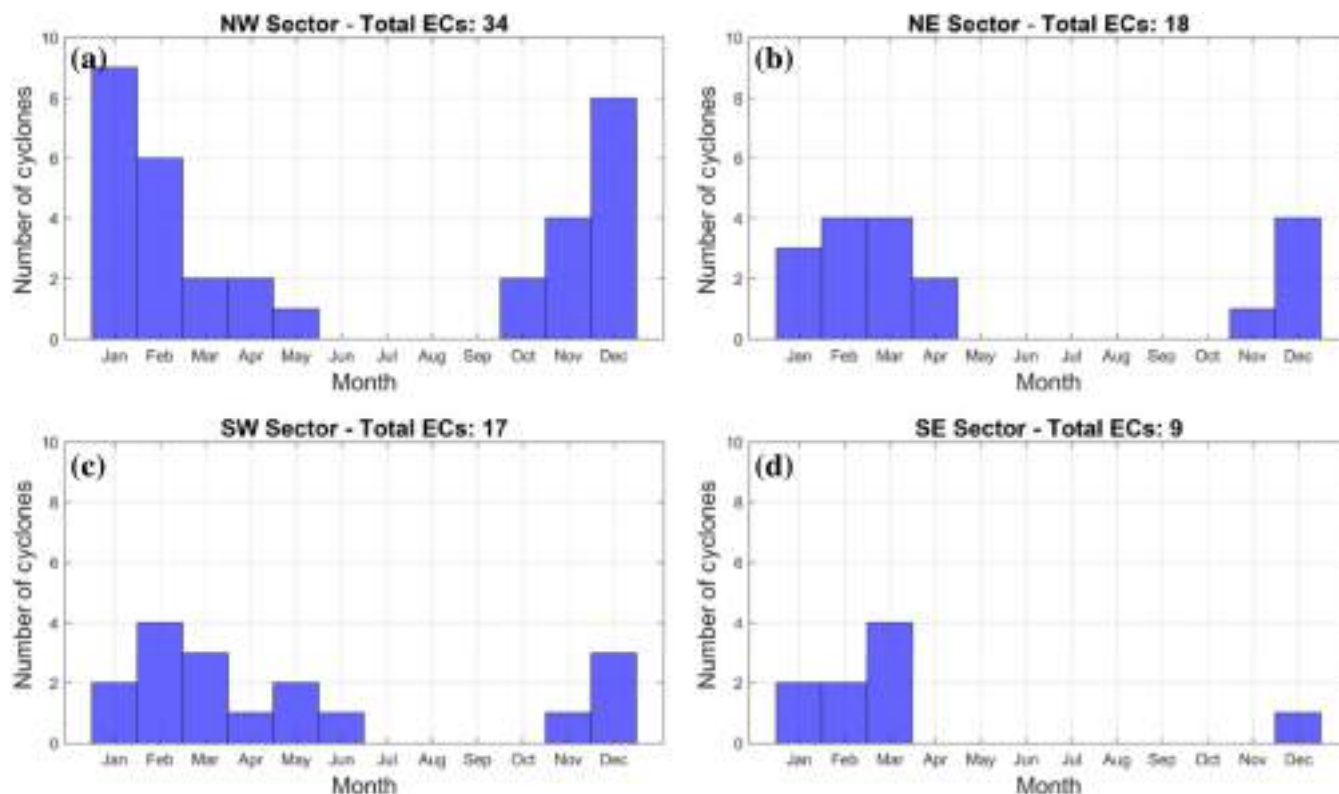


FIGURE 7 Seasonal distribution of explosive cyclones (ECs) in each of the four sectors of the Mediterranean Basin as in Table 1. (a) The NW sector (22 ECs); (b) the NE sector (17 ECs); (c) the SW sector (26 ECs); (d) the SE sector (22 ECs).

further south, mirroring the reduced frequency of occurrence.

A total of 32 cases are in the 1.0–1.1 Bergeron range (41.25%), while, according to the intensity characterization of Zhang et al. (2021), two ECs are identified as “Strong” ($DR > 1.7$ Bergeron), occurring in November 1991 and December 1998, as summarised in Table 4. However, it is worth mentioning that the Mediterranean cyclones have shorter life-spans compared to the Atlantic ones studied by Zhang et al. (2017), as does their permanence over the sea and consequently their intensification.

To complete the picture, Figure 9a illustrates the frequency of ECs in the MB from 1979 to 2020. Notably, no clear linear trend is discernible in the data, as the number of ECs fluctuates significantly over the years. Periods of high activity, such as in the early 1980s and between 2009 and 2012, contrast with years of reduced or no activity, underscoring the variability in EC occurrences rather than a consistent increase or decrease over time. This variability suggests that other factors may be influencing EC formation beyond long-term climatic trends. Figure 9b shows the average magnitude of ECs, reaching a maximum peak in 2004 with an average value of 1.57 Bergeron. In 2018 another peak was recorded, including the Vaia storm (Davolio et al., 2020, Giovannini et al., 2021), which reached a DR of 1.4 Bergeron.

4.4 | Empirical Orthogonal Function analysis to determine the typical synoptic patterns favouring explosive cyclones

Figures 10 and 11 show the EOF analysis performed for the three datasets mentioned in Section 2.3, the ‘Explosive’, the ‘Random’ and the ‘Intense’. The colourbar indicates the normalized EOF loadings. The EOF scores are not shown because we are interested in the spatial gradients of EOF patterns, and not in the relative importance of the single events, which can, however, be determined by using the sign of the EOF score to retrieve the sign of the pressure variations in the EOF patterns presented here. This is achieved by multiplying the sign of the loading in a particular location by the sign of the score during a particular event.

Figure 10a–c highlights the first three ‘EC EOFs’:

- The first (EOF1, Figure 10a) explains 24.83% of the variance and shows a clear contrast between MSLP over the Scandinavian region and the area covering the Azores and part of North Africa. This pattern resembles a Scandinavian pattern (SCAND), an index that measures the relative strength of the N–S pressure dipole in Europe. During positive (negative) SCAND, southern (northern) Europe experiences wetter (drier) conditions (Barnston

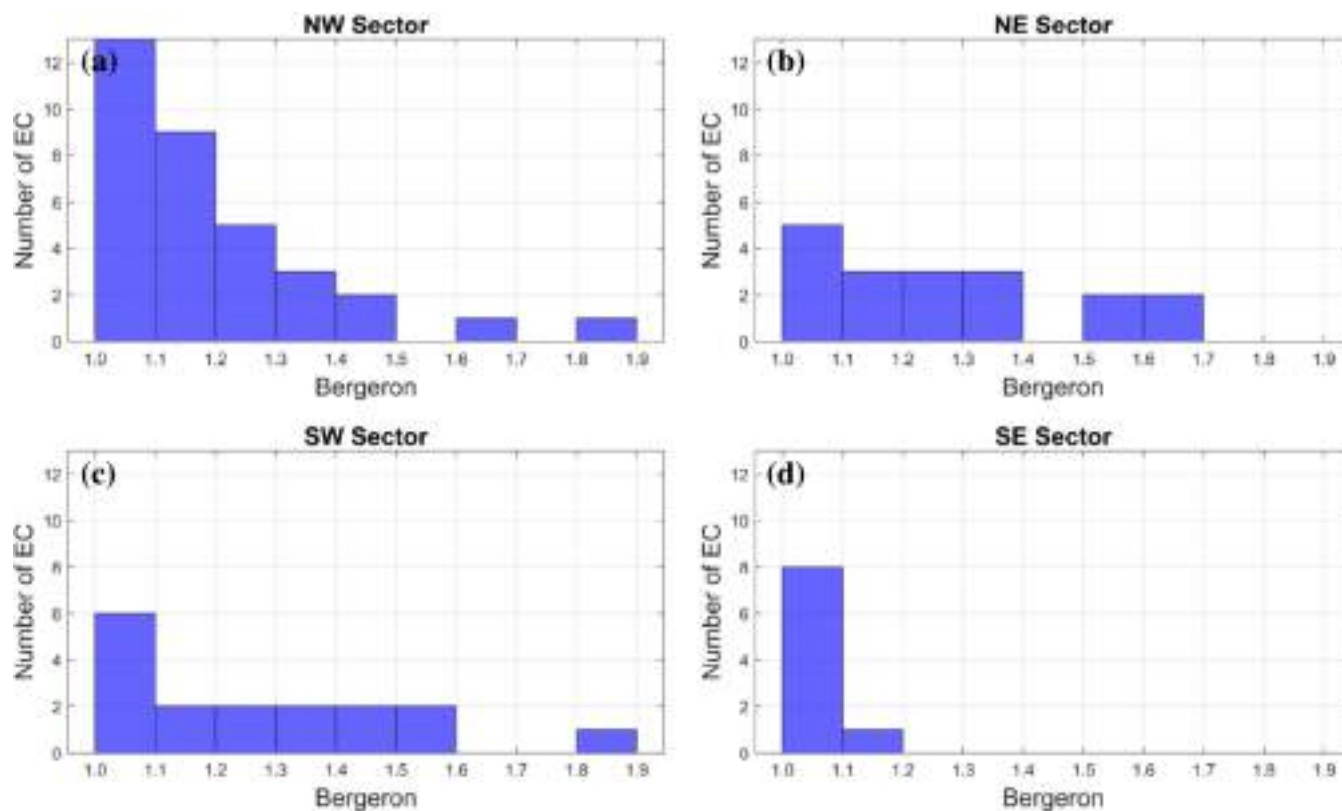


FIGURE 8 Histograms of the frequency distribution of maximum deepening rate in each of the four sectors of the Mediterranean Basin. The x-axis indicates the deepening rate (DR) in Bergeron and the y-axis the frequency of explosive cyclones (ECs).

TABLE 4 Classification of EC events by intensity of deepening.

Intensity	Maximum DR (Bergeron)	Number of ECs	Percentage
Weak	1.00–1.29	58	72.5%
Moderate	1.30–1.69	20	25%
Strong	>1.7	2	2.5%

Abbreviations: DR, deepening rate; EC, explosive cyclone.

& Livezey, 1987; Bueh & Nakamura, 2007). Furthermore, this particular pattern is associated with a higher frequency of cyclones in the MB (Nissen et al., 2010; Ulbrich et al., 2012) with anticyclonic blocking conditions over western Russia and the Scandinavian region.

In the case of negative scores, the SCAND dipole features a high-pressure field in the Scandinavian region and a low pressure in the southern area; for positive scores the dipole is reversed. These two patterns tell us that nearly 25% of the ECs events we identified, during their maximum deepening, are the result of either a circulation

bringing air from the North Atlantic into the Mediterranean, possibly then accounting for cyclogenesis in the area of the Gulf of Genoa, or a circulation favouring the flow from Egypt towards the Aegean Sea.

- The second (EOF2, Figure 10b), explaining the 16.01% of the variance, shows a contrast between Iceland, the western part of Russia and the Atlantic region south of Spain. Thus, depending on the sign of the scores, ECs might enter the MB from the Atlantic, with a trough extending in the Ionian Sea and transporting air from North Africa as well, or alternatively, the circulation might advect air from the Scandinavian region.
- The third EOF (EOF3, Figure 10c), explaining the 10.82% of the variance, highlights strong variations in MSLP (of the same sign) in an area extending from North Africa to the United Kingdom. This area faces another of opposite variation sign covering the Norwegian Sea. In this particular configuration, in case of negative scores, an anticyclone covers the entire western and central Europe, acting as a blocking condition and allowing ECs to enter the Mediterranean from the Scandinavian region.

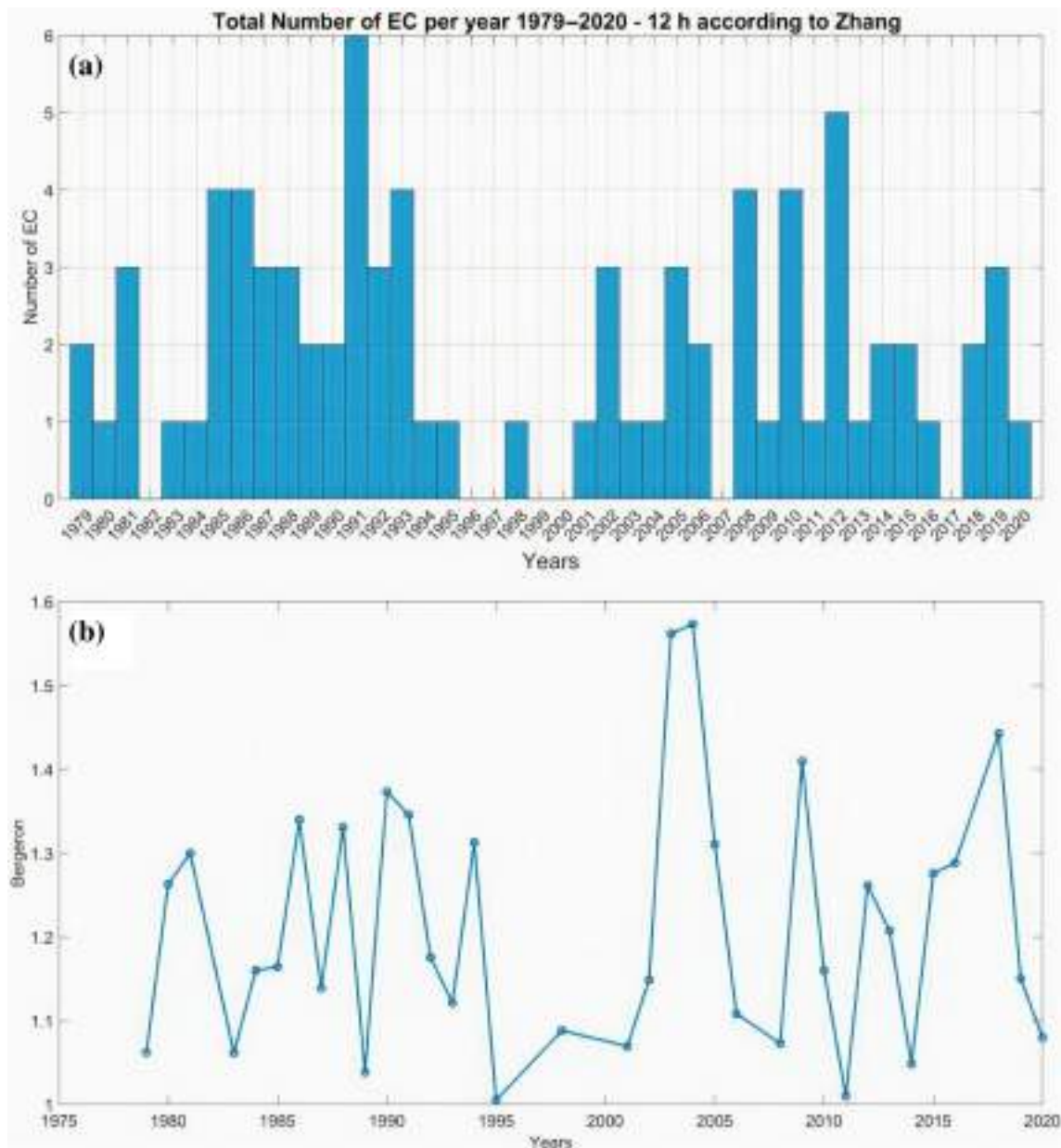


FIGURE 9 (a) Annual distribution of explosive cyclones (ECs) throughout the entire dataset. (b) Average intensity per year in terms of the value of the deepening rate (in Bergeron).

These three patterns explain half of the occurrences of ECs.

Figure 11 depicts the equivalent analysis but for the 'Random' dataset, and it is performed to compare ECs' occurrence patterns to the one of 80 randomly selected cyclones. EOF1, obtained in this case, explaining 21.01% of the variance, resembles the second of the Explosive EOFs. EOF2 (18.42%) is structured as a SCAND pattern, while the EOF3 (11.06%) underlines the role of a blocking condition, typical of the central Mediterranean region (Lionello et al., 2006). Since the two EOF1s do not coincide, the occurrence of ECs in the MB is guided predominantly by

a different synoptic pattern than the one driving randomly selected Mediterranean cyclones.

Through the EOF analysis of the 'Intense' dataset, the plots in Figure 12 reveal that EOF1, accounting for 21.08% of the total variance, displays a synoptic pattern resembling the characteristic dipole of the North Atlantic Oscillation, marked by a strong contrast between the central Atlantic and the Icelandic region. Similarly, EOF2 (representing 13.36% of the variance) shows a structure akin to the SCAND pattern, meanwhile EOF3 reveals a tripole involving the North Atlantic, Western Russia, and Eastern Canada. Notably, the most dominant pattern

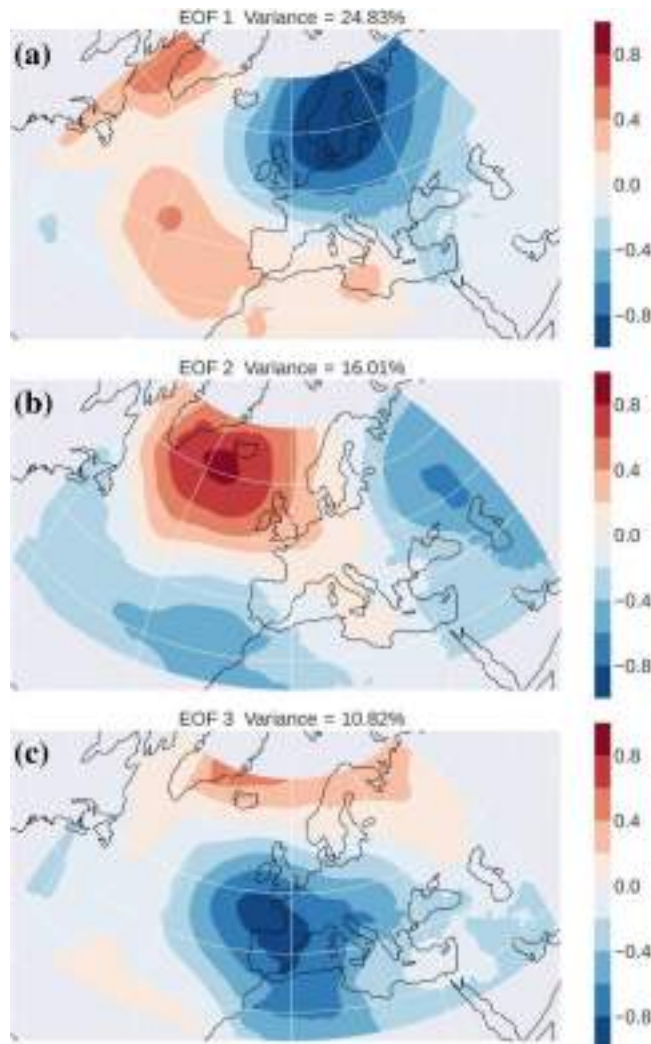


FIGURE 10 First three Empirical Orthogonal Function (EOF) loadings for the 'Explosive' dataset.

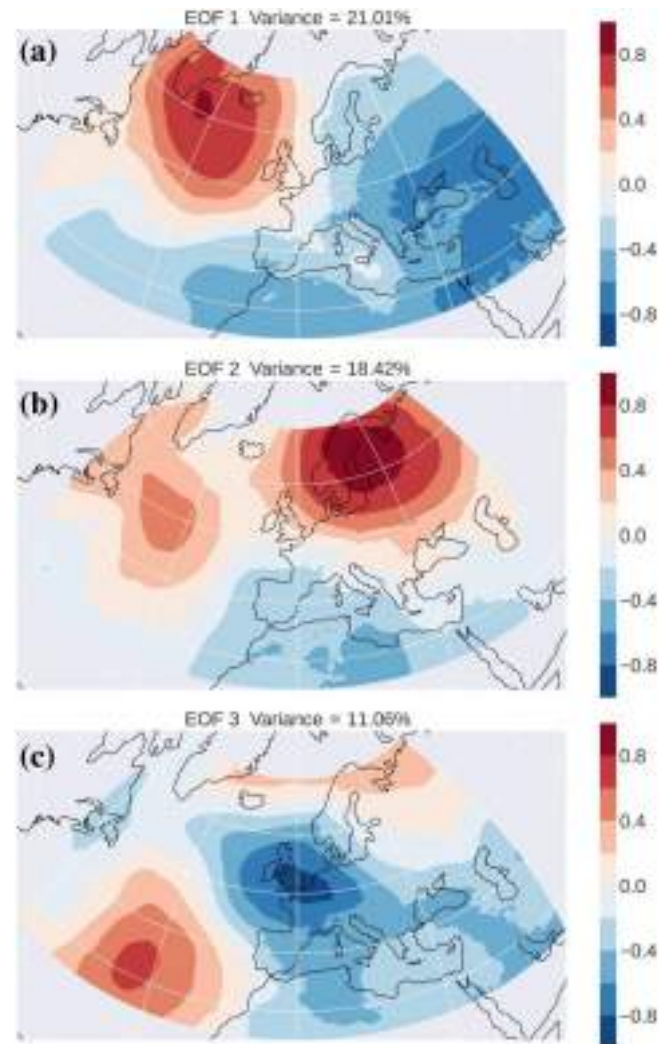


FIGURE 11 First three Empirical Orthogonal Function (EOF) loadings for the 'Random' dataset.

differs, once again, from the one driving the majority of ECs.

4.5 | Composite analysis of upper and lower-level potential vorticity and relative humidity

The following section presents the results of the composite analysis of PV and RH for both ECs and randomly selected non-explosive cyclones.

As depicted in Figure 13a, ECs are characterized by a PV field structured as a streamer of PV anomalies extending from higher latitudes towards the southwestern branch of the cyclone's dry conveyor belt, with maximum mean values of 3.74 potential vorticity units (PVU). This streamer is usually merged with the polar front in

the EDP and it is separated during the mature stage, a pattern that often appears together with blocking conditions associated with the intrusion of high-latitude high-PV air masses at lower latitudes (Kautz et al., 2022). At 500 hPa (Figure 13b), the PV field exhibits a structure consistent with the one observed at 300 hPa, though with lower maximum mean values of 0.88 PVU.

In all ECs PV intrusions are observed to reach levels between 700 and 500 hPa and, under these elongated anomalies, the isentropes are tilted and separated, indicating low static stability (Charney, 1990; Hoskins et al., 1985; Hoskins, 1997; Thorpe, 1985) (not shown).

The PV field at 850 hPa (Figure 13c) reveals peaks of 2.16 PVU near the cyclone centre, likely due to convection and the associated diabatic heating at lower levels, which might be accompanied also by a PV tower (Pang & Fu, 2017; Pang et al., 2022).

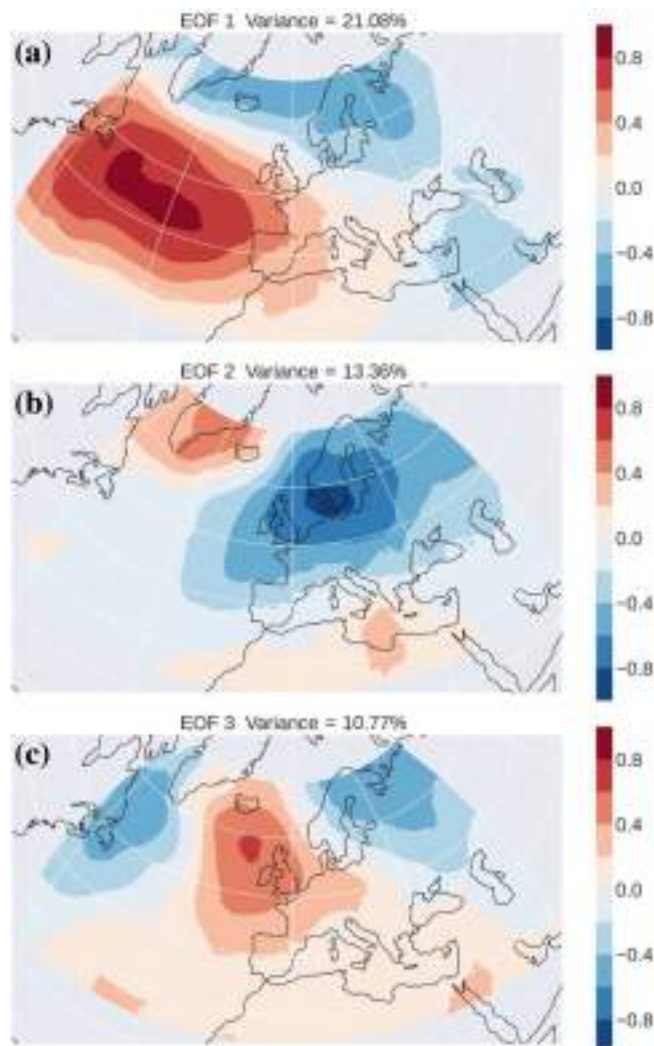


FIGURE 12 First three Empirical Orthogonal Function (EOF) loadings for the 'Intense' dataset.

When comparing these results to those obtained for random cyclones, significant differences emerge. At 300 hPa (Figure 13d), there is a weaker streamer, similar in structure to that of ECs, but the PV anomaly values are notably lower, with maximum mean values of 2.72 PVU. Moreover, the intrusion in random cyclones does not extend as deeply, as evidenced by the much weaker and less structured PV field at 500 hPa (Figure 13e) and the lower-level PV anomalies are not localized around the centre of the cyclone but rather displaced into the northern part of the squared domain (Figure 13f).

In both cases, however, the upper-level PV maximum anomaly is tilted westward with respect to the cyclone centre at the surface, concordant with the well-known theories of baroclinic development (Eady, 1949; Reed, 1955), but in the EC case, the anomaly seems to extend significantly more towards the cyclone's centre.

A similar analysis was conducted to explore the role of SDI in the deepening of ECs (Figure 14). The distinctions between ECs and randomly selected cyclones remain clear, particularly in the upper levels. In the case of ECs, a distinct dry intrusion, characterized by roughly 20% of RH, can be seen penetrating the central area of the cyclone from the northwestern branch at 300 hPa (Figure 14a). A similar pattern is present at 500 hPa (Figure 14b), though with generally higher RH values; however, at the 850 hPa level (Figure 14c), the dry intrusion is no longer apparent.

This structured dry intrusion is absent in the randomly selected cyclones, where the RH patterns at all three levels appear irregular, exhibiting latitudinal variation rather than any clear intrusion. The upper-level intrusion in ECs also closely mirrors the PV anomalies shown in Figure 13a, highlighting the interconnected roles of both processes in driving the explosive intensification of these systems.

4.6 | Frequency distribution of potential vorticity, relative humidity and mean surface latent and sensible heat fluxes

Figure 15 shows the distribution of the number of cyclones in relation to the following variables: minimum RH at (a) 350 hPa and (b) 500 hPa, maximum PV at (c) 350 hPa and (d) 500 hPa, (e) absolute maximum MLHF and (f) absolute maximum MSHF at the surface. The maximum or minimum values of each variable were extrapolated within a radius of 250 km from the position of the cyclone when it reaches its maximum DR (analogously for 80 random cyclones). For each variable the distribution in blue refers to the 80 ECs and the one in yellow to the 80 randomly selected cyclones.

The PV (Figure 15a,b) in the case of ECs spreads across all values, reaching more than 6 PVU, while for random cyclones PV is more concentrated around values lower than 6 PVU, albeit with some sporadic cases that exceed this threshold. Minimum values of RH (Figure 15c,d), although showing similar distributions for the two types of cyclones, presents secondary peaks at values lower than 5% for ECs. Finally, the latent and sensible heat distributions show a similar appearance between ECs and random cyclones, but with a shift of about 100 W/m^2 upwards for ECs.

The highest frequency in the case of ECs is 12 (15%) for PV values at 300 hPa between 5.5 and 6 PVU and 10 (12.50%) between 1.5 and 2 PVU at 500 hPa. Conversely, random cyclones have a maximum of 15 events (18.75%) below 1 PVU at 300 hPa and 21 (26.25%) in the same range at 500 hPa. At 300 hPa, ECs show peaks of 30 events (37.5%) for RH between 0 and 4% and 25 events (31.25%)

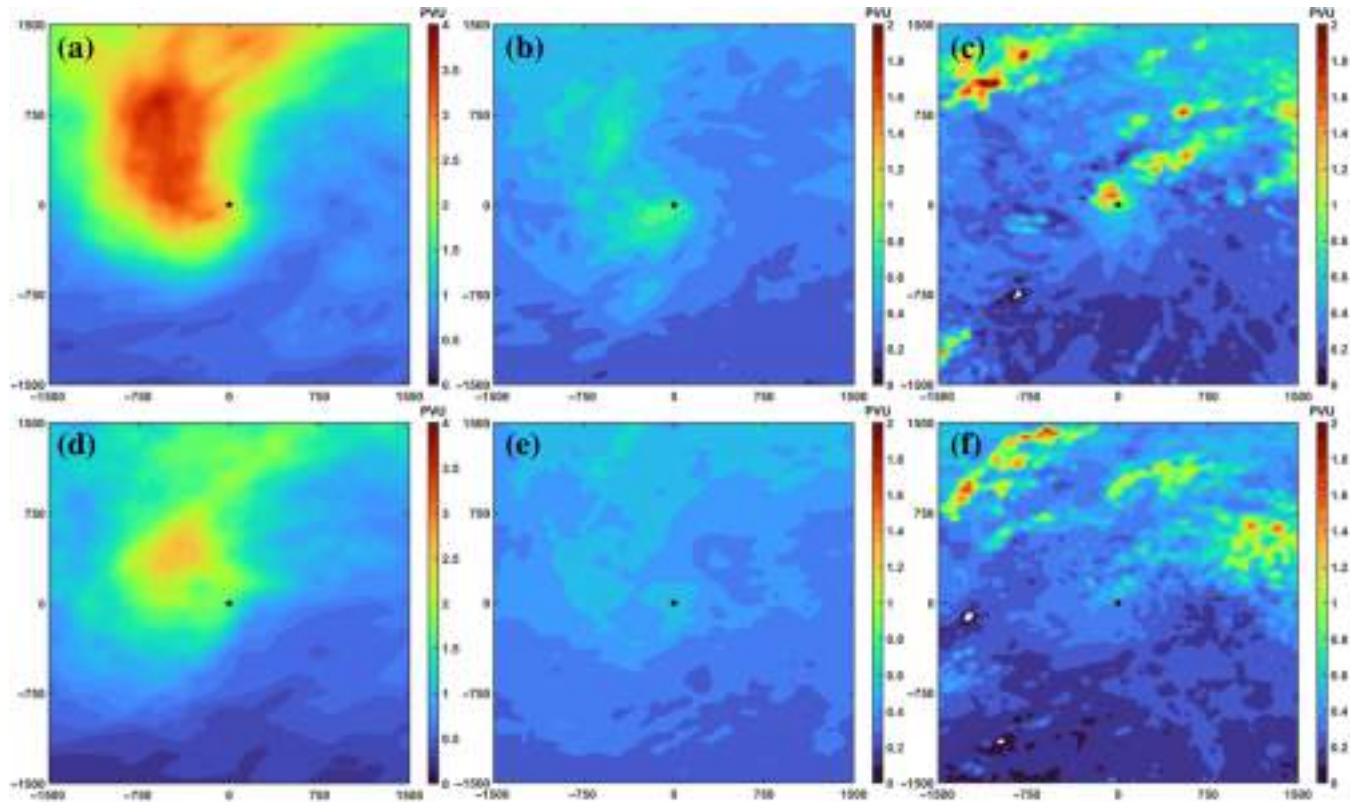


FIGURE 13 Composite analysis for the potential vorticity fields at different pressure levels for explosive cyclones and randomly selected cyclones. Panels (a–c) represent the PV fields for the ECs at 300, 500, and 850 hPa, respectively. Panels (d–f) depict the corresponding PV fields for random cyclones at the same pressure levels (300, 500, and 850 hPa, respectively). The colour scale represents potential vorticity (PV) in PV units (PVU), where warmer colours (reds and yellows) indicate higher PV values associated with stronger cyclonic activity, while cooler colours (blues) represent lower PV values. Stars mark the cyclone centres in each panel. The x- and y-axes indicate the distance in km from the composite centre of the cyclones.

for RH between 4% and 8%. In the same ranges, the random cyclones are limited to 17 (21.25%) and 14 (17.5%) events, respectively.

When investigating the role of diabatic heating and therefore of surface latent and sensible heat fluxes, a drastically different distribution between the two types of cyclones is not evident. In particular, as shown in Figure 15e,f, the ECs tend to present a flow higher in magnitude at the air–sea interface, with the highest frequency of events, 13 (16.25%), in the range $240\text{--}280\text{ W}\cdot\text{m}^{-2}$ for the MLHF distribution, compared to the random ones which register a maximum of 13 (16.25%) but in the range $120\text{--}160\text{ W}\cdot\text{m}^{-2}$. Similarly, in the case of MSHF, the respective maxima are 19 (23.75%) between 120 and $160\text{ W}\cdot\text{m}^{-2}$ for the EC and 17 (21.25%) between 40 and $80\text{ W}\cdot\text{m}^{-2}$ for the random ones.

In summary, ECs display distinct atmospheric and surface characteristics compared to randomly selected cyclones. In terms of PV, ECs exhibit a broader range of high values, exceeding 6 PVU, while random cyclones are concentrated around lower PV values. This suggests that ECs involve stronger upper-level dynamics and more

intense cyclonic activity. Regarding RH, ECs tend to have lower values, with noticeable peaks below 5%, particularly at 300 hPa, indicating the presence of drier air in the upper atmosphere, caused by stronger subsidence or the entrainment of dry air, as explored in Section 4.5. The distribution of latent and sensible heat fluxes between the two types of cyclones is more similar, although ECs consistently show higher magnitudes. This suggests that ECs are more influenced by surface heat fluxes, which may support their explosive development. However, the distinction between ECs and random cyclones is less evident when focusing solely on surface heat fluxes, indicating that diabatic processes may play a role in both, but their contributions are more pronounced in ECs.

5 | DISCUSSION AND CONCLUSIONS

This study exploits for the first time a high-resolution reanalysis dataset (ERA5) to build a climatology of ECs in the MB, investigating the frequency, the spatial and

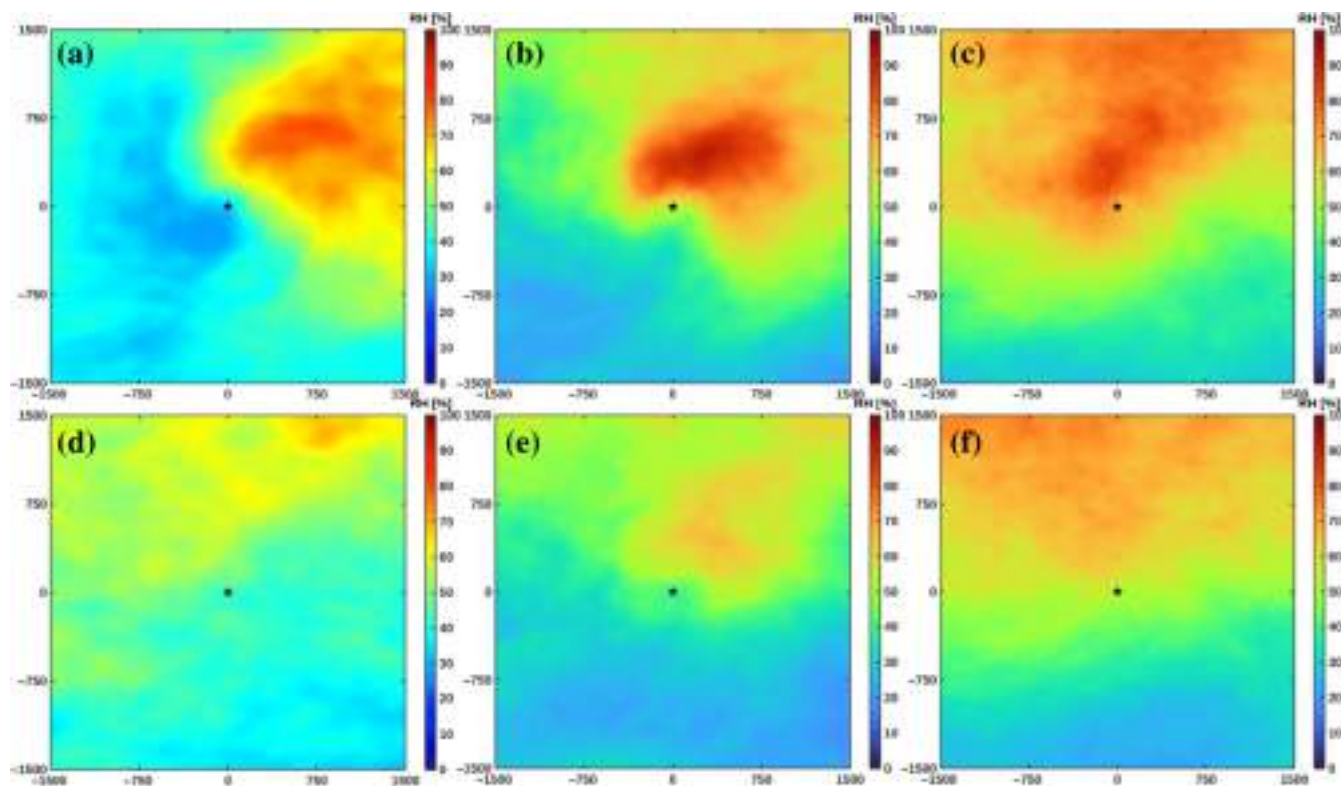


FIGURE 14 Composite analysis for the relative-humidity (RH) fields at different pressure levels for explosive cyclones (ECs) and randomly selected cyclones. Panels (a–c) represent the RH fields for the ECs at 300, 500, and 850 hPa, respectively. Panels (d–f) depict the corresponding RH fields for random cyclones at the same pressure levels. Stars mark the cyclone centres in each panel.

temporal distribution, as well as the most common atmospheric configurations triggering their explosive deepening.

The climatological analysis produced a smaller number of ECs (80 in total) with respect to previous studies, in particular that of Kouroutzoglou et al. (2011), in which over 200 ECs were identified. There are several reasons for this discrepancy:

- The use of ERA5 Reanalysis data, which present a significantly higher spatiotemporal resolution ($0.25^\circ \times 0.25^\circ$, hourly) than the data used in Kouroutzoglou et al., 2011 ($2.5^\circ \times 2.5^\circ$, six-hourly).
- The employment of a new cyclone dataset involving the combination of 10 different, already tested algorithms (Flaounas et al., 2023).
- The chosen spatial domain is reduced with respect to Kouroutzoglou et al., 2011. They considered an area embedding the western part of the MB, including the Gulf of Biscay, that is subjected to the passage of intense cyclones, but with development occurring in the Atlantic and which enter the Mediterranean only for a short time span. In our study we focus exclusively on events that undergo an EDP in the MB.
- In computing the DR Kouroutzoglou et al. (2011) used the formula by Sander and Gyakum (1980), which is referenced to a latitude of 60° N, while in our case, the DR is referenced to a latitude of 45° N. This translates into an overall overestimation of the DR values by Kouroutzoglou et al. (2011), according to Equation (3).
- In our latitudes, particularly in northern Africa, atmospheric tides can play a pivotal role in misleading the DR algorithm into classifying some cyclones as explosive (1 Bergeron or more). For this reason, we filtered out these data, as the intensification of these cyclones is not driven by intrinsic physical factors related to cyclogenesis, but by external environmental conditions with periodic oscillation in CSLP and factors unrelated to the cyclone itself. This phenomenon is especially true in northern Africa, downstream of the Atlas Mountains, where the topographic gradient induces increased vorticity and cyclone intensification. When coinciding with certain phases of atmospheric tides, this can lead to a resemblance (in terms of Bergeron) to EC, leading to false detection of ECs.

The main findings are the following:

1. A total of 80 ECs were recorded throughout the entire dataset, mainly developing in distinct geographical

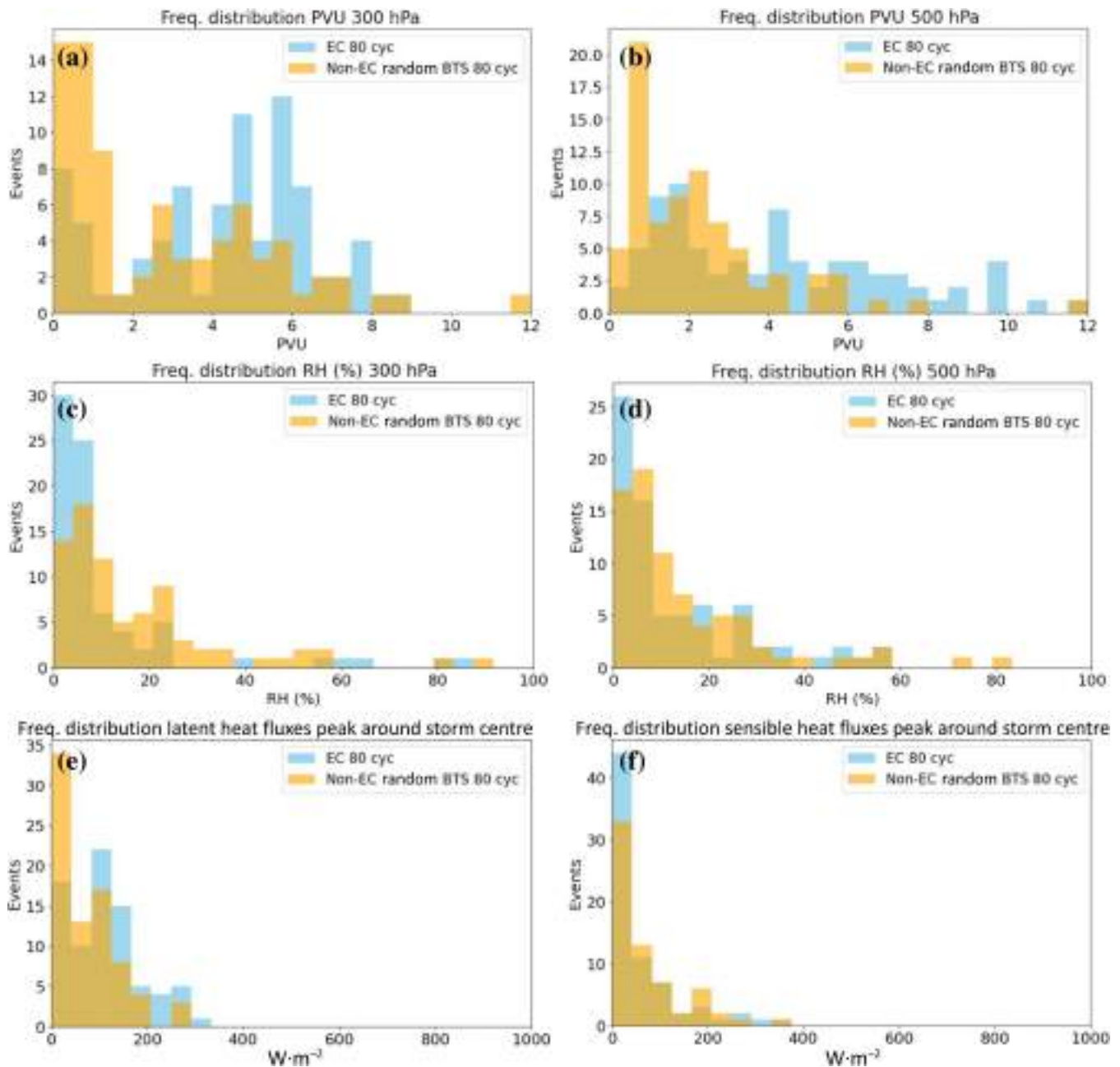


FIGURE 15 Distribution of the number of events recorded according to the variables analysed. The blue histograms represent the distribution of ECs, the yellow ones represent 80 random cyclones. (a) PV at 300 hPa; (b) PV at 500 hPa; (c) RH at 350 hPa; (d) RH at 500 hPa; (e) mean surface latent heat flux; (f) mean surface sensible heat flux.

regions. The NW sector seems to be the most favourable area, with nearly half of the total number of occurrences, possibly due to orographic deformation of the flow of baroclinic waves from the Atlantic generated by the Alps, which results in a strong and sudden variation of relative vorticity (Buzzi et al., 2020; Buzzi & Tibaldi, 1978; Speranza et al., 1985). The region experiences the passage of cyclones with genesis typical of the Genoa Low (Buzzi et al., 2020; Buzzi & Tibaldi, 1978), but also of cyclones originating near

the Balearic Islands and the Tyrrhenian Sea (thus with characteristics different from the Genoa Low) that often approach this region as already powerful weather systems due to their previous intensification over the sea.

2. In all the four geographical sectors, ECs have their peaks in winter or early spring, from December to March.
3. Two ECs (2.5% of the total number) are classified as 'Strong', reaching an absolute maximum DR value of

1.87 Bergeron. Both originate in North Africa, with tracks crossing the entire Mediterranean, in one case northeastward and in the other northwestward.

4. The maximum DR in nearly 80% of the cases is reached over the sea, indicative of the possible role of air–sea interaction processes in the intensification of ECs. We have shown how the heat provided by the sea is one of the factors that influence the explosive deepening of cyclones.
5. As a result of the EOF analysis, the SCAND pattern explains most of the variance and it features blocking conditions over western Russia and the Scandinavian region during cyclone evolution. It also accounts for those cyclones originating from Atlantic baroclinic waves, which, in this configuration, can be elongated towards Morocco and interact with the Atlas Mountains, causing ECs to start deepening and then to proceed towards the Ionian Sea and the Levantine Basin. The EOF analysis reveals that ECs show statistically different synoptic patterns from those of randomly selected cyclones and another pool of particularly intense cyclones from the dataset.
6. The composite analysis of PV and RH shows a distinctive PV anomaly streamer extending from higher latitudes towards the southwestern branch of the cyclone's dry conveyor belt, reaching maximum values of 3.74 PVU at 300 hPa. The intrusions of PV and RH are consistent with each other, penetrating up to 500 hPa in the occlusion area, with a well-defined pattern, while at 850 hPa, convection and diabatic heating contribute to PV peaks near the cyclone centre. In contrast, random cyclones exhibit weaker and less organized PV anomalies, with lower values and shallower intrusions, lacking the defining features of ECs. The upper-level PV anomalies in ECs elongate significantly deeper towards the cyclone's centre, emphasizing their role in the intensification process.
7. The values of 300 and 500 hPa PV among ECs are on average higher than those reached by 80 randomly selected cyclones, and values of RH at the same levels are lower in the case of ECs, further suggesting the importance of PV anomalies and SDI in the ECs' EDP. The diabatic heating role does not seem to differ for ECs and random cyclones, even though ECs tend to present slightly more intense fluxes at the air–sea interface.

Shorter time spans for the calculation of DR were tested during the study, but due to contamination by solar semidiurnal atmospheric tides, the analysis has been carried out with a 12-hour time step. Nevertheless, it is important to point out again, that if cyclone differential pressure data were available and used in the analyses, higher temporal resolutions of ECs would be made possible, also allowing

those with much shorter life cycles than 12 hours to be explored properly. The ERA5 dataset used in this study can, in principle, be used to extract the cyclone differential pressure p . However, this is beyond the scope of the present study.

A similar analysis can be conducted to determine how these patterns are going to be modified by the climate change in the future, evaluating the different scenarios from different high-resolution climatological model runs. Hence, the climatology resulting from this study will be available to the whole scientific community.

ACKNOWLEDGEMENTS

This work was supported by National Centre for HPC, Big Data and Quantum Computing – PNRR Project, funded by the European Union – Next Generation EU and is a contribution to the COST action CA19109 Med-Cyclones (European network for Mediterranean cyclones in weather and climate, CA19109); Special Project ASIM-CPL founded by ECMWF. Dr Antonio Ricchi (University of L'Aquila/CETEMPS) is funded by PON-DM1062 Project. Special thanks to Emmanouil Flaounas for providing the initial tracking dataset. We thank the reviewers for their comments that greatly improved the manuscript.

CONFLICT OF INTEREST STATEMENT

The authors declare that the research was conducted in the absence of any commercial or financial relationships that could be construed as a potential conflict of interest.

DATA AVAILABILITY STATEMENT

The data that support the findings of this study are available from the corresponding author upon reasonable request.

ORCID

Cosimo Enrico Carniel  <https://orcid.org/0000-0001-9902-3410>

Antonio Ricchi  <https://orcid.org/0000-0002-7061-8442>

Rossella Ferretti  <https://orcid.org/0000-0003-1630-2698>


Gabriele Curci  <https://orcid.org/0000-0001-9871-5570>

Mario Marcello Miglietta  <https://orcid.org/0000-0003-2898-1595>

Marco Reale  <https://orcid.org/0000-0003-1004-8203>

Silvio Davolio  <https://orcid.org/0000-0001-8704-1814>

Dino Zardi  <https://orcid.org/0000-0002-3573-3920>

Lakshmi Kantha  <https://orcid.org/0000-0002-4968-7101>

REFERENCES

- Ahmadi-Givi, F., Graig, G.C. & Plant, R.S. (2004) The dynamics of a midlatitude cyclone with very strong latent-heat release.

- Quarterly Journal of the Royal Meteorological Society, 130, 295–323. Available from: <https://doi.org/10.1256/qj.02.226>
- Allen, J.T., Pezza, A.B. & Black, M.T. (2010) Explosive cyclogenesis: a global climatology comparing multiple reanalyses. *Journal of Climate*, 23, 6468–6484. Available from: <https://doi.org/10.1175/2010JCLI3437.1>
- Anthes, R.A., Kuo, Y.-H. & Gyakum, J.R. (1983) Numerical simulations of a case of explosive marine cyclogenesis. *Monthly Weather Review*, 111, 1174–1188. Available from: [https://doi.org/10.1175/1520-0493\(1983\)111<1174:NSOACO>2.0.CO;2](https://doi.org/10.1175/1520-0493(1983)111<1174:NSOACO>2.0.CO;2)
- Barnston, A.G. & Livezey, R.E. (1987) Classification, seasonality and persistence of low-frequency atmospheric circulation patterns. *Monthly Weather Review*, 115, 1083–1126. Available from: [https://doi.org/10.1175/1520-0493\(1987\)115<1083:CSAPOL>2.0.CO;2](https://doi.org/10.1175/1520-0493(1987)115<1083:CSAPOL>2.0.CO;2)
- Bosart, L.F. & Lin, S.C. (1984) A diagnostic analysis of the Presidents' day storm of February 1979. *Monthly Weather Review*, 112, 2148–2177. Available from: [https://doi.org/10.1175/1520-0493\(1984\)112<2148:ADAOTP>2.0.CO;2](https://doi.org/10.1175/1520-0493(1984)112<2148:ADAOTP>2.0.CO;2)
- Bueh, C. & Nakamura, H. (2007) Scandinavian pattern and its climatic impact. *Quarterly Journal of the Royal Meteorological Society*, 133, 2117–2131. Available from: <https://doi.org/10.1002/qj.173>
- Buzzi, A., Davolio, S. & Fantini, M. (2020) Cyclogenesis in the lee of the Alps: a review of the theories. *Bulletin of Atmospheric Science and Technology*, 1, 433–457. Available from: <https://doi.org/10.1007/s42865-020-00021-6>
- Buzzi, A. & Tibaldi, S. (1978) Cyclogenesis in the lee of the Alps: a case study. *Quarterly Journal of the Royal Meteorological Society*, 104, 271–287. Available from: <https://doi.org/10.1002/qj.49710444004>
- Charney, J.G. (1990) On the scale of atmospheric motions. In: Lindzen, R.S., Lorenz, E.N. & Platzman, G.W. (Eds.) *The atmosphere — a challenge*. Boston, MA: American Meteorological Society. Available from: https://doi.org/10.1007/978-1-944970-35-2_14
- Conte, M. (1986) The meteorological “bomb” in the Mediterranean: a synoptic climatology. *Rivista di Meteorologia Aeronautica*, XLVI 314, 121–130.
- Conte, M., Piervitali, E. & Colacino, M. (1997) The meteorological bomb in the Mediterranean. *INM/WMO International Symposium on Cyclones and Hazardous Weather in the Mediterranean MMA/UIB*; 283–287.
- Covey, C., Dai, A., Marsh, D. & Lindzen, R.S. (2011) The surface-pressure signature of atmospheric tides in modern climate models. *Journal of the Atmospheric Sciences*, 68(3), 495–514. Available from: <https://doi.org/10.1175/2010JAS3560.1>
- Davolio, S., Della Fera, S., Laviola, S., Miglietta, M.M. & Levizzani, V. (2020) Heavy precipitation over Italy from the Mediterranean storm “Vaia” in October 2018: assessing the role of an Atmospheric River. *Monthly Weather Review*, 148, 3571–3588. Available from: <https://doi.org/10.1175/MWR-D-20-0021.1>
- Dawson, A. (2016) eofs: a library for EOF analysis of meteorological, oceanographic, and climate data. *Journal of Open Research Software*, 4(1), e14. Available from: <https://doi.org/10.5334/jors.122>
- Eady, E.T. (1949) Long waves and cyclone waves. *Tellus*, 1(3), 33–52. Available from: <https://doi.org/10.3402/tellusa.v1i3.8507>
- Emanuel, K.A., Fantini, M. & Thorpe, A.J. (1987) Baroclinic instability in an environment of small stability to slantwise moist convection. Part I: two-dimensional models. *Journal of the Atmospheric Sciences*, 44, 1559–1573. Available from: [https://doi.org/10.1175/1520-0469\(1987\)044<1559:BIIAEO>2.0.CO;2](https://doi.org/10.1175/1520-0469(1987)044<1559:BIIAEO>2.0.CO;2)
- Flaounas, E., Kelemen, F.D., Wernli, H., Gaertner, M.A., Reale, M., Sanchez-Gomez, E. et al. (2018). Assessment of an ensemble of ocean-atmosphere coupled and uncoupled regional climate models to reproduce the climatology of Mediterranean cyclones. *Climate Dynamics*, 51(3), 1023–1040. Available from: <https://doi.org/10.1007/s00382-016-3398-7>
- Flaounas, E., Davolio, S., Raveh-Rubin, S., Pantillon, F., Miglietta, M.M., Gaertner, M.N. et al. (2022) Mediterranean cyclones: current knowledge and open questions on dynamics, prediction, climatology and impacts. *Weather and Climate Dynamics*, 3(1), 173–208. Available from: <https://doi.org/10.5194/wcd-3-173-2022>
- Flaounas, E., Aragão, L., Bernini, L., Dafis, S., Doiteau, B., Flocas, H. et al. (2023). A composite approach to produce reference datasets for extratropical cyclone tracks: application to Mediterranean cyclones. *Weather and Climate Dynamics*, 4(3), 639–661. Available from: <https://https://doi.org/10.5194/wcd-4-639-2023>
- Gall, R. (1976) A comparison of linear baroclinic instability theory with the eddy statistics of a general circulation model. *Journal of the Atmospheric Sciences*, 33, 349–373. Available from: [https://doi.org/10.1175/1520-0469\(1976\)033<0349:ACOLBI>2.0.CO;2](https://doi.org/10.1175/1520-0469(1976)033<0349:ACOLBI>2.0.CO;2)
- Giovannini, L., Davolio, S., Zaramella, M., Zardi, D. & Borga, M. (2021) Multi-model convection-resolving simulations of the October 2018 Vaia storm over Northeastern Italy. *Atmospheric Research*, 253, 105455. Available from: <https://doi.org/10.1016/j.atmosres.2021.105455>
- Gyakum, J.R. (1983) On the evolution of the QE II storm. II: dynamic and thermodynamic structure. *Monthly Weather Review*, 111(6), 1156–1173. Available from: [https://doi.org/10.1175/1520-0493\(1983\)111<1156:OTEOTI>2.0.CO;2](https://doi.org/10.1175/1520-0493(1983)111<1156:OTEOTI>2.0.CO;2)
- Hersbach, H., Bell, B., Berrisford, P., Hirahara, S., Horányi, A., Muñoz-Sabater, J. et al. (2020). The ERA5 global reanalysis. *Quarterly Journal of the Royal Meteorological Society*, 146(730), 1999–2049. Portico. Available from: <https://doi.org/10.1002/qj.3803>
- Hersbach, H., Bell, B., Berrisford, P., Biavati, G., Horányi, A., Muñoz Sabater, J. et al. (2023) ERA5 hourly data on single levels from 1940 to present. *Copernicus Climate Change Service (C3S) Climate Data Store (CDS)*. Available from: <https://doi.org/10.24381/cds.adbb2d47>
- Hoskins, B. (1997) A potential vorticity view of synoptic development. *Meteorological Applications*, 4(4), 325–334. Available from: <https://doi.org/10.1017/S1350482797000716>
- Hoskins, B.J., McIntyre, M.E. & Robertson, A.W. (1985) On the use and significance of isentropic potential vorticity maps. *Quarterly Journal of the Royal Meteorological Society*, 111(470), 877–946. Available from: <https://doi.org/10.1002/qj.49711147002>
- Karacostas, T.S. & Flocas, A.A. (1983) The development of the bomb over the Mediterranean area in Climat méditerranéen et ressources en eau. *Première partie. La Météorologie Paris*, 34, 351–358.
- Kautz, L.A., Martius, O., Pfahl, S., Pinto, J.G., Ramos, A.M., Sousa, P.M. et al. (2022) Atmospheric blocking and weather extremes over the Euro-Atlantic sector—a review. *Weather and Climate*

- Dynamics*, 3(1), 305–336. Available from: <https://doi.org/10.5194/wcd-3-305-2022>
- Kouroutzoglou, J., Flocas, H.A., Keay, K., Simmonds, I. & Hatzaki, M. (2011) Climatological aspects of explosive cyclones in the Mediterranean. *International Journal of Climatology*, 31(12), 1785–1802. Available from: <https://doi.org/10.1002/joc.2203>
- Lagouvardos, K., Kotroni, V. & Defer, E. (2007) The 21–22 January 2004 explosive cyclogenesis over the Aegean Sea: observations and model analysis. *Quarterly Journal of the Royal Meteorological Society: A Journal of the Atmospheric Sciences, Applied Meteorology and Physical Oceanography*, 133(627), 1519–1531. Available from: <https://doi.org/10.1002/qj.121>
- Liberato, M.L.R., Pinto, J.G., Trigo, R.M., Ludwig, P., Ordóñez, P., Yuen, D. et al. (2013) Explosive development of winter storm Xynthia over the subtropical North Atlantic Ocean. *Natural Hazards and Earth System Sciences*, 13(9), 2239–2251. Available from: <https://doi.org/10.5194/nhess-13-2239-2013>
- Lionello, P., Bhend, J., Buzzi, A., Della-Marta, P.M., Krichak, S.O., Jansà, A. et al. (2006) Chapter 6: cyclones in the Mediterranean region: climatology and effects on the environment. In: *Developments in earth and environmental sciences*, Vol. 4. Amsterdam: Elsevier, pp. 325–372. Available from: [https://doi.org/10.1016/S1571-9197\(06\)80009-1](https://doi.org/10.1016/S1571-9197(06)80009-1)
- Lionello, P., Trigo, I.F., Gil, V., Liberato, M.L.R., Nissen, K.M., Pinto, J.G. et al. (2016) Objective climatology of cyclones in the Mediterranean region: a consensus view among methods with different system identification and tracking criteria. *Tellus A: Dynamic Meteorology and Oceanography*, 68(1), 29391. Available from: <https://doi.org/10.3402/tellusa.v68.29391>
- Manobianco, J. (1989) Explosive East Coast cyclogenesis over the west-central North Atlantic Ocean: a composite study derived from ECMWF operational analysis. *Monthly Weather Review*, 117, 2365–2383. Available from: [https://doi.org/10.1175/1520-0493\(1989\)117<2365:EECCOT>2.0.CO;2](https://doi.org/10.1175/1520-0493(1989)117<2365:EECCOT>2.0.CO;2)
- Miglietta, M.M., Carnevale, D., Levizzani, V. & Rotunno, R. (2021) Role of moist and dry air advection in the development of Mediterranean tropical-like cyclones (medicanes). *Quarterly Journal of the Royal Meteorological Society*, 147(735), 876–899. Available from: <https://doi.org/10.1002/qj.3951>
- Miglietta, M.M. & Rotunno, R. (2019) Development mechanisms for Mediterranean tropical-like cyclones (medicanes). *Quarterly Journal of the Royal Meteorological Society*, 145(721), 1444–1460. Available from: <https://doi.org/10.1002/qj.3503>
- Mullen, S.L. & Baumhefner, D.P. (1988) Sensitivity of numerical simulations of explosive oceanic cyclogenesis to changes in physical parameterizations. *Monthly Weather Review*, 116(11), 2289–2329. Available from: [https://doi.org/10.1175/1520-0493\(1988\)116<2289:SONSOE>2.0.CO;2](https://doi.org/10.1175/1520-0493(1988)116<2289:SONSOE>2.0.CO;2)
- Murray, R.J. & Simmonds, I. (1991a) A numerical scheme for tracking cyclone centres from digital data. *Australian Meteorological Magazine*, 39(3), 155–166.
- Murray, R.J. & Simmonds, I. (1991b) A numerical scheme for tracking cyclone centres from digital data. Part II: application to January and July general circulation model simulations. *Australian Meteorological Magazine*, 39(3), 167–180.
- Nissen, K.M., Leckebusch, G.C., Pinto, J.G., Renggli, D., Ulbrich, S. & Ulbrich, U. (2010) Cyclones causing wind storms in the Mediterranean: characteristics, trends and links to large-scale patterns. *Natural Hazards and Earth System Sciences*, 10(7), 1379–1391. Available from: <https://doi.org/10.5194/nhess-10-1379-2010>
- Pang, H. & Fu, G. (2017) Case study of potential vorticity tower in three explosive cyclones over Eastern Asia. *Journal of the Atmospheric Sciences*, 74(5), 1445–1454. Available from: <https://doi.org/10.1175/JAS-D-15-0330.1>
- Pang, H., Fu, G. & Lu, C. (2022) Structure of the potential vorticity of an explosive cyclone over the eastern Asian region in late November 2013. *Journal of Ocean University of China*, 21, 253–263. Available from: <https://doi.org/10.1007/s11802-022-4787-7>
- Reader, M.C. & Moore, G.K. (1995) Stratosphere-troposphere interactions associated with a case of explosive cyclogenesis in the Labrador Sea. *Tellus A*, 47(5), 849–863. Available from: <https://doi.org/10.1034/j.1600-0870.1995.00124.x>
- Reale, M., Cabos Narvaez, W.D., Cavicchia, L., Conte, D., Coppola, E., Flaounas, E. et al. (2022) Future projections of Mediterranean cyclone characteristics using the Med-CORDEX ensemble of coupled regional climate system models. *Climate Dynamics*, 1–24, 2501–2524. Available from: <https://doi.org/10.1007/s00382-021-06018-x>
- Reale, M., Liberato, M.L., Lionello, P., Pinto, J.G., Salon, S. & Ulbrich, S. (2019) A global climatology of explosive cyclones using a multi-tracking approach. *Tellus A: Dynamic Meteorology and Oceanography*, 71(1), 1611340. Available from: <https://doi.org/10.1080/16000870.2019.1611340>
- Reed, R.J. (1955) A study of a characteristic type of upper-level frontogenesis. *Journal of Atmospheric Sciences*, 12(3), 226–237. Available from: [https://doi.org/10.1175/1520-0469\(1955\)012<0226:ASOACT>2.0.CO;2](https://doi.org/10.1175/1520-0469(1955)012<0226:ASOACT>2.0.CO;2)
- Roebber, P.J. (1984) Statistical analysis and updated climatology of explosive cyclones. *Monthly Weather Review*, 112(8), 1577–1589. Available from: [https://doi.org/10.1175/1520-0493\(1984\)112<1577:SAAUCO>2.0.CO;2](https://doi.org/10.1175/1520-0493(1984)112<1577:SAAUCO>2.0.CO;2)
- Sanders, F. (1986) Explosive cyclogenesis in the west-central North Atlantic Ocean, 1981–84. Part I: composite structure and mean behavior. *Monthly Weather Review*, 114(10), 1781–1794. Available from: [https://doi.org/10.1175/1520-0493\(1986\)114<1781:ECITWC>2.0.CO;2](https://doi.org/10.1175/1520-0493(1986)114<1781:ECITWC>2.0.CO;2)
- Sanders, F. & Gyakum, J.R. (1980) Synoptic-dynamic climatology of the “bomb”. *Monthly Weather Review*, 108(10), 1589–1606. Available from: [https://doi.org/10.1175/1520-0493\(1980\)108<1589:SDCOT>2.0.CO;2](https://doi.org/10.1175/1520-0493(1980)108<1589:SDCOT>2.0.CO;2)
- Schindelegger, M. & Ray, R.D. (2014) Surface pressure tide climatologies deduced from a quality-controlled network of barometric observations. *Monthly Weather Review*, 142(12), 4872–4889. Available from: <https://doi.org/10.1175/MWR-D-14-00217.1>
- Simmonds, I. & Murray, R.J. (1999). Southern Extratropical Cyclone Behavior in ECMWF Analyses during the FROST Special Observing Periods. *Weather and Forecasting*, 14(6), 878–891. Available from: [https://doi.org/10.1175/1520-0434\(1999\)014<0878:SECBIE>2.0.CO;2](https://doi.org/10.1175/1520-0434(1999)014<0878:SECBIE>2.0.CO;2)
- Sinclair, V.A., Rantanen, M., Haapanala, P., Räisänen, J. & Järvinen, H. (2020) The characteristics and structure of extra-tropical cyclones in a warmer climate, *Weather Clim. Dynamis*, 1, 1–25. Available from: <https://doi.org/10.5194/wcd-1-1-2020>
- Speranza, A., Buzzi, A., Trevisan, A. & Malguzzi, P. (1985) A theory of deep cyclogenesis in the lee of the Alps. Part I: modifications of baroclinic instability by localized topography. *Journal*

- of the *Atmospheric Sciences*, 42(14), 1521–1535. Available from: [https://doi.org/10.1175/1520-0469\(1985\)042<1521:ATODCI>2.0.CO;2](https://doi.org/10.1175/1520-0469(1985)042<1521:ATODCI>2.0.CO;2)
- Thorpe, A.J. (1985) Diagnosis of balanced vortex structure using potential vorticity. *Journal of the Atmospheric Sciences*, 42(4), 397–406. Available from: [https://doi.org/10.1175/1520-0469\(1985\)042<0397:DOBVSU>2.0.CO;2](https://doi.org/10.1175/1520-0469(1985)042<0397:DOBVSU>2.0.CO;2)
- Uccellini, L.W., Keyser, D., Brill, K.F. & Wash, C.H. (1985). The Presidents' Day Cyclone of 18–19 February 1979: Influence of Upstream Trough Amplification and Associated Tropopause Folding on Rapid Cyclogenesis. *Monthly Weather Review*, 113(6), 962–988. Available from: [https://doi.org/10.1175/1520-0493\(1985\)113<0962:tpdcof>2.0.co;2](https://doi.org/10.1175/1520-0493(1985)113<0962:tpdcof>2.0.co;2)
- Uccellini, L.W. (1990) Processes contributing to the rapid development of extratropical cyclones. *Extratropical Cyclones: The Erik Palmén Memorial*, 81–105. Available from: https://doi.org/10.1007/978-1-944970-33-8_6
- Ulbrich, U., Lionello, P., Belušić, D., Jacobeit, J., Knippertz, P., Kuglitsch, F.G. et al. (2012) Climate of the Mediterranean: synoptic patterns, temperature, precipitation, winds, and their extremes. In: *The climate of the Mediterranean Region*. Amsterdam: Elsevier, pp. 301–346. Available from: <https://doi.org/10.1016/B978-0-12-416042-2.00005-7>
- Uppala, S.M., Kållberg, P.W., Simmons, A.J., Andrae, U., Bechtold, V.D.C., Fiorino, M. et al. (2005) The ERA-40 re-analysis. *Quarterly Journal of the Royal Meteorological Society: A Journal of the Atmospheric Sciences, Applied Meteorology and Physical Oceanography*, 131(612), 2961–3012. Available from: <https://doi.org/10.1256/qj.04.176>
- Wang, C.C. & Rogers, J.C. (2001) A composite study of explosive cyclogenesis in different sectors of the North Atlantic. Part I: cyclone structure and evolution. *Monthly Weather Review*, 129(6), 1481–1499. Available from: [https://doi.org/10.1175/1520-0493\(2001\)129<1481:ACSOEC>2.0.CO;2](https://doi.org/10.1175/1520-0493(2001)129<1481:ACSOEC>2.0.CO;2)
- Wash, C.H., Hale, R.A., Dobos, P.H. & Wright, E.J. (1992) Study of explosive and nonexplosive cyclogenesis during FGGE. *Monthly Weather Review*, 120(1), 40–51. Available from: [https://doi.org/10.1175/1520-0493\(1992\)120<0040:SOEANC>2.0.CO;2](https://doi.org/10.1175/1520-0493(1992)120<0040:SOEANC>2.0.CO;2)
- Zehnder, J.A. & Keyser, D. (1991) The influence of interior gradients of potential vorticity on rapid cyclogenesis. *Tellus A*, 43(3), 198–212. Available from: <https://doi.org/10.1034/j.1600-0870.1991.t01-2-00003.x>
- Zhang, S., Fu, G., Lu, C. & Liu, J. (2017) Characteristics of explosive cyclones over the Northern Pacific. *Journal of Applied Meteorology and Climatology*, 56(12), 3187–3210. Available from: <https://doi.org/10.1175/JAMC-D-16-0330.1>
- Zhang, S., Liu, C., Xu, J., Zhang, S., Tang, R., Huang, Z. et al. (2021) Physical process contributions to the development of a super explosive cyclone over the Gulf stream. *Frontiers in Earth Science*, 9, 722555. Available from: <https://doi.org/10.3389/feart.2021.722555>

SUPPORTING INFORMATION

Additional supporting information can be found online in the Supporting Information section at the end of this article.

How to cite this article: Carniel, C.E., Ricchi, A., Ferretti, R., Curci, G., Miglietta, M.M., Reale, M. et al. (2024) A high-resolution climatological study of explosive cyclones in the Mediterranean region: Frequency, intensity and synoptic drivers. *Quarterly Journal of the Royal Meteorological Society*, 150(765), 5561–5582. Available from: <https://doi.org/10.1002/qj.4889>